Table 1
Characteristics of identified amino acid variants in *TRPM4*.*

No.	Patient	Exon	Nucleotide	Amino Acid	Effect	Genotype	Other variant(s) in susceptibility genes	SIFT | PPH-2	dbSNP141 database id	EUR_AF (1000 genomes) (%)	EVS_UAMAF (%)	AllelicFreq_NFE (ExAC) (%)	ECG morphology	Phenotype
1.1	35	6	c.755 G>A	R252H [16]	missense_variant	Heterozygous	0	deleterious(0.01) | possibly_damaging(0.772)	rs146564314	0	0.63	0.818	RBBB	type 2 AVB 2°
1.2	36	6	c.755 G>A	R252H [16]	missense_variant	Heterozygous	0	deleterious(0.01) | possibly_damaging(0.772)	rs146564314	0	0.63	0.818	LBBB	type 2 AVB 2°
1.3	37	6	c.755 G>A	R252H [16]	missense_variant	Heterozygous	0	deleterious(0.01) | possibly_damaging(0.772)	rs146564314	0	0.63	0.818	Normal	type 2 AVB 2°
2	13	7	c.858 G>A	T286T	splice_region_variant & synonymous_variant	Heterozygous	1 (*GJA5*)	|		0	0.00	0.001	Normal	AVB 3°
3	9	9	c.1127 T>C	I376T	missense_variant	Heterozygous	0	deleterious(0.02) | benign(0.323)		0	0.00	0	RBBB + LAHB	Normal
4	4	11	c.1294 G>A	A432T [7,15,16]	missense_variant	Heterozygous	2 (*TRPM4* and *RYR2*)	deleterious(0) | probably_damaging(0.97)	rs201907325	0.13	0.10	0.056	LBBB	AVB 3°
5	24	11	c.1324 C>T	R442C	missense_variant	Heterozygous	1 (*SCN5A*)	deleterious(0) | probably_damaging(0.996)	rs148867331	0	0.02	0.018	RBBB + LAHB	Normal
6.1	21	12	c.1682 A>C	D561A [16]	missense_variant	Heterozygous	1 (*SCN1B*)	tolerated(0.22) | benign(0.086)	rs56355369	0.13	0.55	0.618	RBBB	AVB 3°
6.2	28	12	c.1682 A>C	D561A [16]	missense_variant	Heterozygous	1 (*SCN5A*)	tolerated(0.22) | benign(0.086)	rs56355369	0.13	0.55	0.618	RBBB	AVB 3°
7	4	13	c.1744 G>A	G582S [15,16]	missense_variant & splice_region_variant	Heterozygous	2 (*TRPM4* and *RYR2*)	tolerated(0.34) | benign(0.037)	rs172149856	0.13	0.10	0.060	LBBB	AVB 3°
8.1	38	16	c.2209 G>A	G737R [15]	missense_variant & splice_region_variant	Heterozygous	0	tolerated(0.59) | benign(0.007)	rs145847114	0.4	0.17	0.180	LBBB	AVB 1° + type 2 AVB 2°
8.2	39	16	c.2209 G>A	G737R [15]	missense_variant & splice_region_variant	Heterozygous	0	tolerated(0.59) | benign(0.007)	rs145847114	0.4	0.17	0.180	RBBB + LPHB	AVB 1°
9	40	17	c.2531 G>A	G844D* [7,16]	missense_variant	Homozygous	0	tolerated(0.2) | probably_damaging(0.945)	rs200038418	0.13	0.16	0.431	RBBB + LAHB	AVB 2/1, 3/1
10	41	17	c.2561 A>G	Q854R [15,16]	missense_variant	Heterozygous	0	tolerated(0.29) | benign(0.029)	rs172155862	0.26	0.12	0.289	LAD	type 2 AVB 2°
11	3	18	c.2674 C>T	R892C	missense_variant	Heterozygous	3 (TNNI3K, *SCN1B* and *RYR2*)	deleterious(0) | probably_damaging(0.985)	rs147854826	0	0.10	0.081	Normal	AVB 3°
12	10	18	c.2675 G>A	R892H	missense_variant	Heterozygous	1 (*SCN5A*)	deleterious(0.02) | benign(0.252)		0	0.00	0	RBBB + LAHB	AVB 3°
13.1	42	24	c.3611 C>T	P1204L [15,16]	missense_variant	Heterozygous	0	tolerated(0.21) | unknown(0)	rs150391806	0.13	0.33	0.505	Normal	AVB 3°
13.2	43	24	c.3611 C>T	P1204L [15,16]	missense_variant	Heterozygous	0	tolerated(0.21) | unknown(0)	rs150391806	0.13	0.33	0.505	RBBB + LAHB	AVB 1°

RBBB: Right Bundle Branch Block; LBBB: Left Bundle Branch Block; LAHB: Left Anterior HemiBlock; LPHB: Left Posterior HemiBlock; LAD: Left Axis Deviation; AVB: AtrioVentricular Block
Variants already described in some articles are noted: [7] Liu et al., [16] Stallmeyer et al., [15] Liu et al.
* The patient 40 has been identified as homozygous for this variant (G844D).

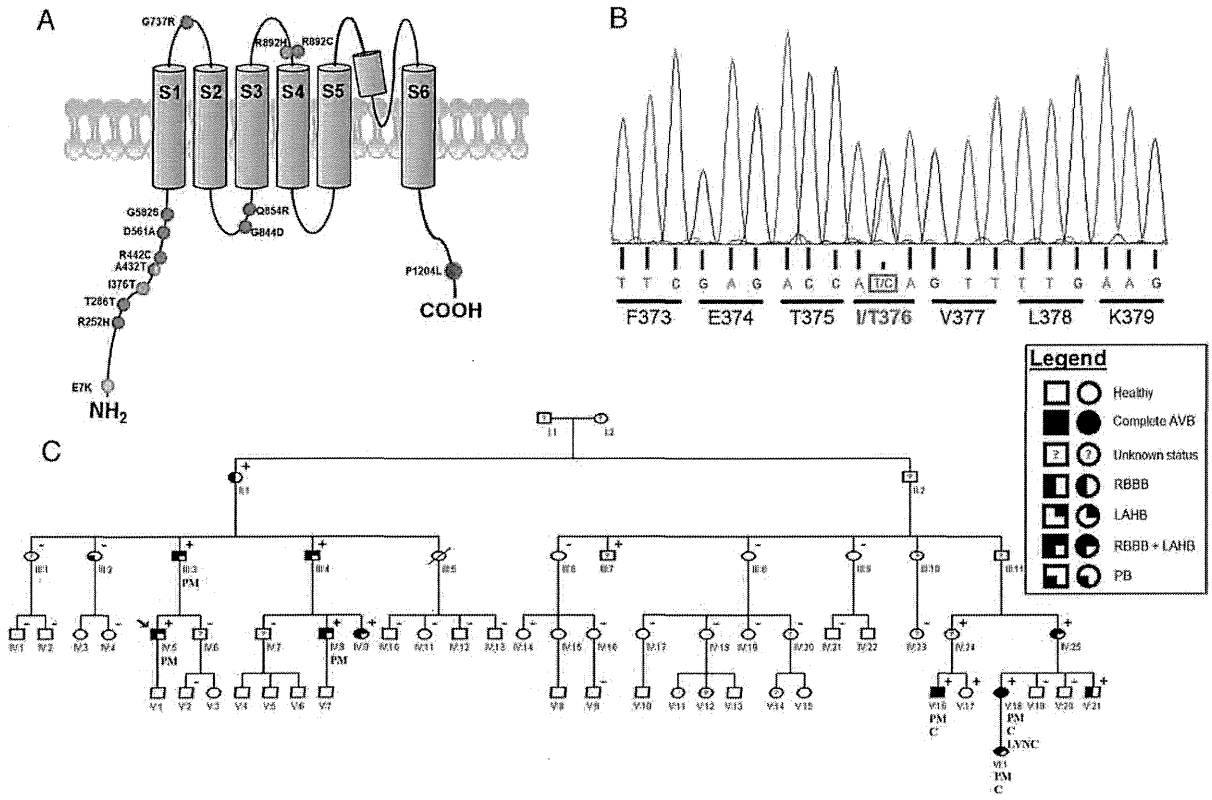

Fig. 1. The *TRPM4*-p.I376T variant is responsible for PFHBI. (A) Distribution of rare coding variation detected among 95 patients with PCCD in the TRPM4 channel. Novel variants are shown in red, low-frequency ones in blue. The two rare variants previously reported as causing PFHBI [6,7] are indicated in green. (B) Capillary sequencing of the exon 9 of *TRPM4* for the patient 9 confirms the presence of a novel variant resulting in the p.I376T substitution. (C) Family tree of patient 9 (the proband, IV-5). Plus symbols (+) denotes p.I376T mutation carriers and minus symbol (−) non-carriers. 'PM' indicates patients implanted with a pacemaker, 'LVNC' stands for Left Ventricular Non-Compaction and 'C' indicates congenital forms of conduction defects.

conduction defects (and one with Small Fiber Neuropathy; see Supplemental Table 1).

3.2. TRPM4 is the most frequently affected gene

The most frequently affected gene is *TRPM4*, with a total of 13 rare variants identified and then validated by capillary sequencing (Table 1). Seven of these variants (54%) are located in the intracellular N-terminal region (Fig. 1a). Two of them – p.I376T and p.R892H – are absent from public databases and thus considered as novel.

The *TRPM4*-p.I376T missense variant, which resides in the intracellular N-terminal domain (Fig. 1a), was identified in the male patient 9 (Fig. 1b). No other rare variant altering any other known PCCD-susceptibility genes could be identified in this patient. The affected

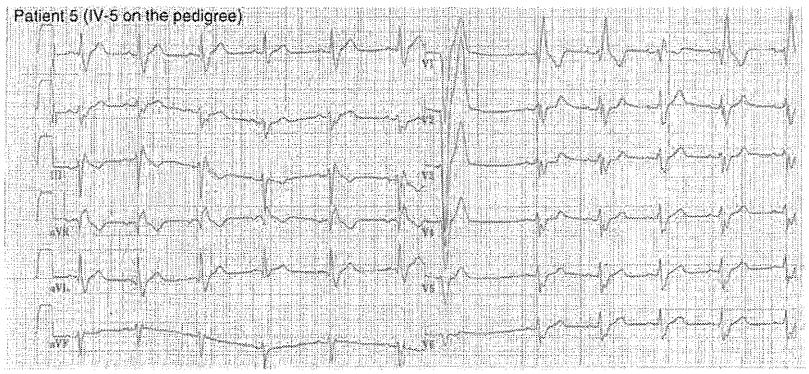

Fig. 2. The ECG profile of the proband IV-5. This patient presented with a heart rate of 69 bpm, a complete right bundle branch block and a left anterior hemiblock enlarging the QRS complex to 170 ms. ECG was recorded at a 25 mm/s paper speed and 0,1 mV/mm signal amplitude. A premature ventricular beat can also be observed in the first QRS complex of the precordial lead.

Table 2
Clinical data of the affected family members.

Patient no.	Age at last clinical examination	Heart rate (bpm)	PR (ms)	QRS (ms)	QTc (ms)	ECG morphology	Conduction	PM (age)
IV-5 (proband)	32	69	160	170	474	RBBB + LAHB	Normal	32 y.o.
II-1	85	63	138	126	439	RBBB	Normal	
III-2	60	81	170	128	439	PB	Normal	
III-3	50	35	200	120	336	RBBB + LAHB	type 2 AVB 2°	50 y.o.
III-4	51	55	188	158	439	RBBB + LAHB	Normal	
IV-8	33	59	180	168	436	RBBB + LAHB	Normal	31 y.o.
IV-9	25	76	170	166	504	RBBB + LAHB	Normal	
IV-25	40	74	200	130	434	RBBB + LAHB	AVB 1°	
V-16	8	45		148	398	RBBB + LAHB	type 2 AVB 2° and AVB 3°	at birth
V-18*	12	35				LBBB	AVB 3°	at birth
V-21	11	73	136	123	441	RBBB	Normal	
VI-1	0	62	144	90	439	RBBB + LAHB	type 2 AVB 2°	8-month-old

RBBB: Right Bundle Branch Block; LAHB: Left Anterior HemiBlock; PB: Parietal Block; LBBB: Left Bundle Branch Block; AVB: AtrioVentricular Block.
* This patient presented with a left ventricular non-compaction phenotype.

amino acid is located in a highly conserved region across vertebrates as indicated by its *Genomic Evolutionary Rate Profiling* score [26] of 4.24 (Supplemental Fig. 2). It is predicted as deleterious (0.02) by SIFT [20] but benign (0.323) by PolyPhen-2 (PPH-2) [21].

The *TRPM4*-p.R892H variant has been identified in the patient 10, who presents with a complete AVB. We found that the same patient also carries a rare missense variant in *SCN5A* (p.A572D), suggesting that the *TRPM4*-p.R892H variant alone may not be responsible for the observed cardiac conduction defects. Another substitution affecting the same amino acid - *TRPM4*-p.R892C - was detected in a second patient (patient 3), but was also reported at an MAF below 1% in public databases (Table 1).

3.3. Familial recruitment

Patient nine carrying the *TRPM4*-p.I376T variant (patient IV-5 in the pedigree) was diagnosed with complete RBBB and LAHB (Fig. 2) and was implanted with a PM for conduction disorders at the age of 32. Familial investigation has been undertaken for this patient, indicated as the proband IV-5 on Fig. 1c.

A total of 96 family members could be identified, among which 57 have been recruited (Fig. 1c). Twelve patients were diagnosed with conduction defects, of which six (50%) were implanted with a PM (Table 2). Ten of the 12 patients presented with RBBB, among which 8 showed LAHB. The eleventh patient (V-18) exhibited an isolated LBBB; the last one (III-2) PB (Table 2).

Two patients (V-16 and VI-1) exhibiting at birth 2:1 AVB with RBBB and LAHB QRS morphology alternant with complete AVB were classified as patients with a congenital AVB, as well as the patient V-18 who exhibited a permanent complete AVB with a 30 bpm ventricular escape rhythm with a complete LBBB QRS morphology. This patient also met the magnetic resonance image diagnostic criteria for a left ventricular non compaction while echocardiography had failed to identify this phenotype (Fig. 1c). Note that the patient IV-6 presented with minor conduction defects (QRS duration of 118 ms) and a slight left axis deviation (−14°), but was not considered as affected following our criteria and thus was classified as 'unknown'.

Age at last clinical evaluation (34 ± 25 vs 22 ± 16, ns), PR (169 ± 24 ms vs 138 ± 20 ms, $P < 0.001$), QRS (138 ± 26 ms vs 88 ± 13 ms, $P < 10^{-10}$) and QTc (438 ± 42 ms vs 417 ± 22 ms, $P < 0.05$) durations were higher in the affected members compared to non-affected members while the heart rate was lower in the affected group (61 ± 16 bpm vs 77 ± 16 bpm, $P < 0.01$) (Table 3).

The novel *TRPM4*-c.T1127C variant (TRPM4-p.I376T) was systematically assessed among family members (Fig. 1c). We were able to test 39 family members: 10 out of the 11 affected patients that we tested (90.9%) carried the *TRPM4* variant versus only 1 out of 21 unaffected family members (4.8%). The twelfth patient suffering from cardiac conduction disease (patient VI-1) was born in 2012 and thus was not genotyped given his young age. The two-point logarithm of the odds ratio (LOD) score was estimated at 4.1182 for this locus - assuming a disease allele frequency of 0.01%, a disease penetrance of 80% and a recombination fraction of 0%. These findings indicate a genotype–phenotype cosegregation in an autosomal dominant manner in this large French family affected by PFHBI. The patient III-2, while appearing as a phenocopy, may show conduction defects caused by a previous anterior myocardial infarct while the patient V-17 (born in 1994) was still young at recruitment time (17 years old), which may explain the absence of conductance disturbance for this variant carrier. This patient will be subjected to regular clinical follow-up since carrying the putative causal variant may confer higher risk to develop PCCD with aging.

3.4. The p.I376T variant induces a gain-of-function of TRPM4 channel

To investigate the effect of the p.I376T variant on TRPM4 expression levels, we performed Western blot and cell surface biotinylation experiments. As previously published [27], we observed that the TRPM4 channel is expressed in fully and core glycosylated forms (Fig. 3). In the presence of the p.I376T variant, we observed an increased expression of these two forms at the cell membrane (Fig. 3). The functional consequences of the p.I376T variant were investigated using the whole-cell configuration of the patch-clamp technique. As reported by our group [28], TRPM4 currents recorded over time show two distinct phases (Fig. 4a). After the membrane rupture, a fast transient phase is observed; it is followed by a plateau phase in which the current amplitude is stable (Fig. 4a). The functional characterization of the p.I376T variant shows in this condition an increase of TRPM4 current densities in both transient and plateau phases, (Table 4, Fig. 4b, c and d).

Table 3
Comparison of age at last clinical evaluation, heart rate, PR, QRS and QTc durations between affected and unaffected members of the family.

	Affected	Unaffected	p value (affected vs unaffected)
Patients (N)	12	45	
Age (years)	34 ± 25	24 ± 16	NS
Heart rate (bpm)	61 ± 16	75 ± 17	<0.01
PR (ms)	169 ± 24	140 ± 21	<0.001
QRS (ms)	138 ± 26	90 ± 13	$<10^{-10}$
QTc (ms)	438 ± 42	415 ± 24	<0.05

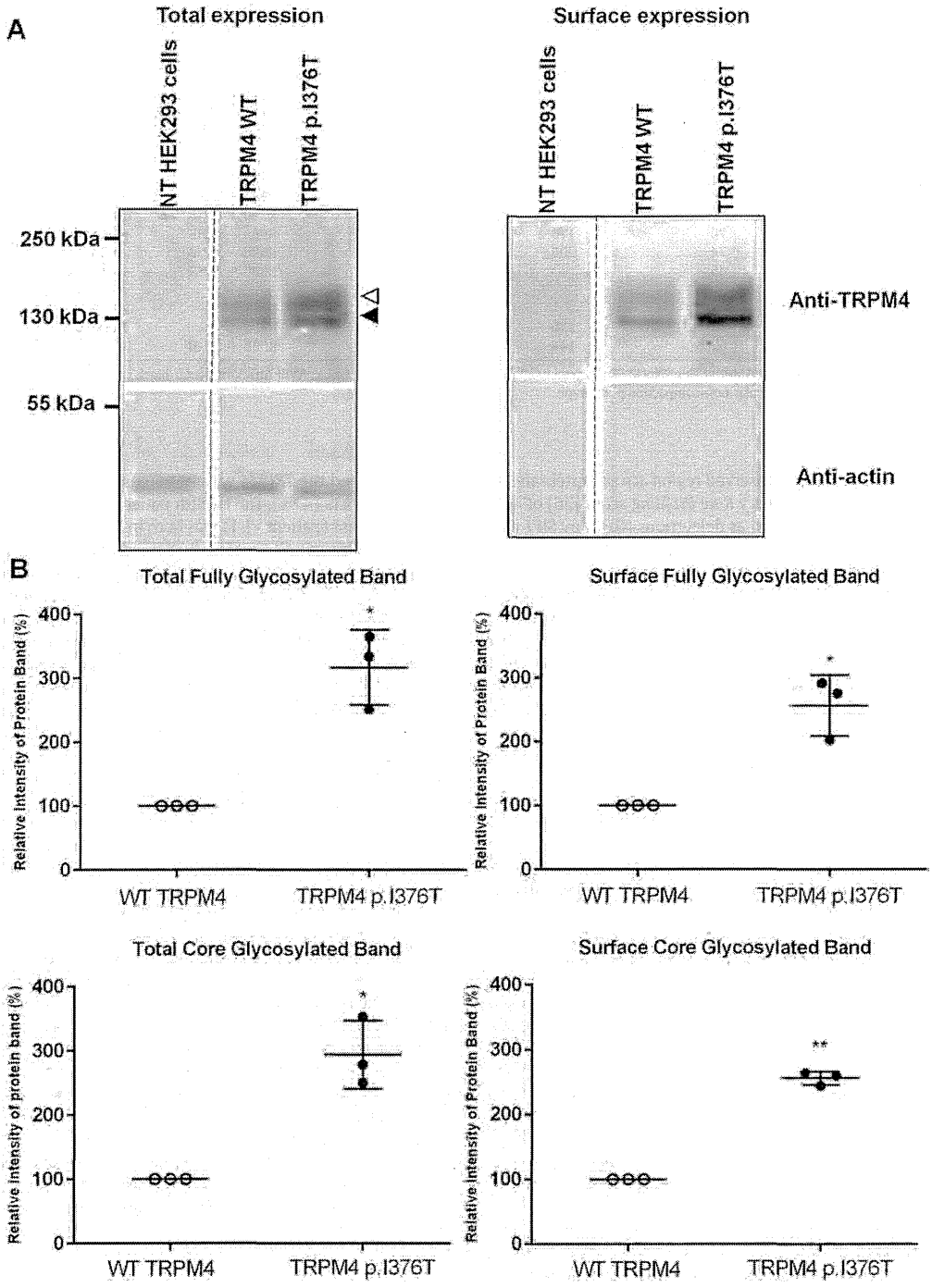

Fig. 3. Expression of the WT and p.I376T TRPM4 channels. (A) Western blots showing the expression of TRPM4 at the total (left panel) and surface levels (right panel) with white and black arrowheads representing fully glycosylated and core-glycosylated forms of TRPM4, respectively. (B) Quantification of the Western blots is shown as relative intensity of protein bands for both fully- and core-glycosylated forms of TRPM4 in each fraction. *P < 0.05, **P < 0.01.

4. Discussion

In the present study, thirteen variants in the *TRPM4* gene were identified using NGS technologies upon screening of a cohort of 95 patients with PCCD. Eleven of these variants were previously listed in at least one of the used public databases. Two of them (p.A432T and p.G844D) were previously reported in familial autosomal conduction block and were shown as deleterious [7]. Five other variants (p.R252H, p.D561A,

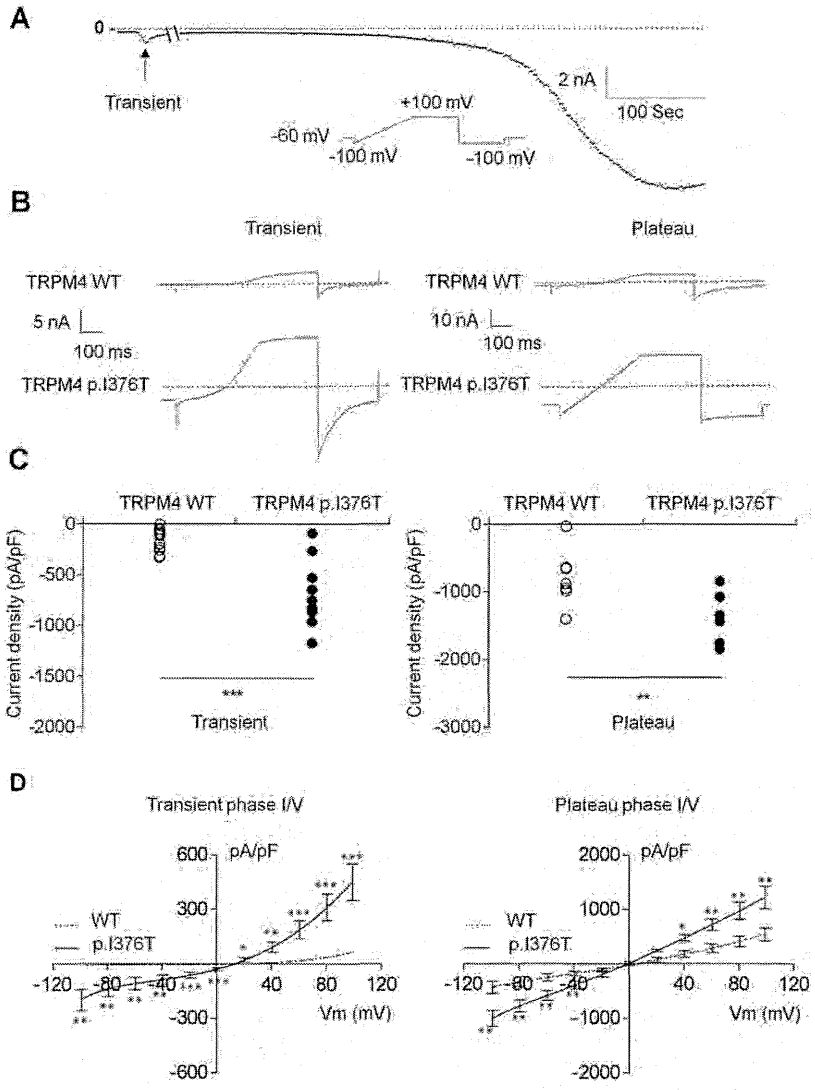

Fig. 4. Whole cell patch clamp recording for the WT and p.I376T TRPM4 channels. (A) Time course recording of the TRPM4 current. (B) Individual current traces of the WT and p.I376T TRPM4 channels recorded as transient and plateau phases. (C) Quantification of current density of the WT and p.I376T TRPM4 channels for both phases. The current densities are measured at the pic current at −100 mV. (D) Current–voltage relationships of the WT and p.I376T TRPM4 channels. *P < 0.05, **P < 0.01, ***P < 0.001.

p.G582S, p.Q854R and p.P1204L) have been reported in sporadic cases presenting with conduction disorders and/or Brugada syndrome [15, 16]. Of interest p.R252H was identified in 3 unrelated patients all of which exhibiting a type 2 second-degree AVB (patients 35, 36 and 37). The four other variants (three missense variants p.R442C, p.G737R and p.R892C and one synonymous variant predicted to affect splicing of the seventh intron p.T286T) have not been causally related to conduction disorders and/or arrhythmia so far.

Another variant, *TRPM4*-p.R892H, is novel since absent from public databases. However, as the patient carrying this variant also carries an *SCN5A*-p.A572D variant, no conclusion could be drawn on the relative pathogenicity of each of these two variants.

The last variant identified in *TRPM4* (p.I376T) is also novel. Familial investigations led to the identification of 96 members including 12 patients with conduction disorders. This is the third largest pedigree diagnosed with PFHBI in which a *TRPM4* mutation significantly segregates in an autosomal dominant manner with the pathology. Thus, this study represents the first NGS-based detection of a *TRPM4* variant that has led to the recruitment of a large 4-generation pedigree from the proband (patient IV-5 on Fig. 1c) carrying the mutation p.I376T. Of interest, the novel variant p.I376T is located in the same intracellular N-terminal domain as the 2 causal variants previously identified in large pedigrees

Table 4
The functional characterization of the I376T variant.

	TRPM4 WT	TRPM4 p.I376T
Current density of Transient Phase (pA/pF)	−161 ± 31 n = 12	−678 ± 113 n = 9
Current density of plateau phase (pA/pF)	−772 ± 138 n = 8	−1390 ± 134 n = 7

(Fig. 1a) [11,18]. Noteworthy, 6 out of the 11 low-frequency variants identified in this study also reside in the same intracellular N-terminal domain, thus suggesting that this domain could be a preferential site for PFHBI causing mutations.

In the present family, a large majority of affected members present with RBBB and anterior hemiblocks, without any LBBB. This pattern is similar to the clinical descriptions of the families previously linked to mutations in *TRPM4* [6,7], which corresponds to the PFHB type IB definition. Our study, in combination with previously published works [6,7, 16] strongly support the prominent role of this cardiac TRP channel in this subtype of conduction disease. The clinical onset of conduction disturbances tends to occur at an early age among affected patients. In particular, the presence of three cases of congenital AVB implanted with a PM during the first year of life also suggests an important role of heritability in disease severity. Furthermore, the observation that these three congenital AVB patients are first- or second-degree relatives suggests that additional genetic factors are strengthening the disease susceptibility in these patients.

Expression and functional analyses were performed using HEK293 cells, in whole-cell patch-clamp configuration and Western blotting. The *TRPM4* p.I376T results in an increased current density that may be caused by an augmented TRPM4 channel expression at the cell surface as previously described [6,7]. The underlying mechanisms leading to conduction block caused by TRPM4 dysfunction are not yet understood. It has been proposed [15,29] that gain-of-function mutations may depolarize the cells of the conduction system, reduce the availability of the cardiac sodium channels and current and thereby alter the normal impulse propagation in Purkinje fibers. This model is consistent with the large QRS complexes observed in PFHBI patients. Conversely, loss-of-function mutations of TRPM4 may lead to a hyperpolarization of the membrane potential, and so reduce cellular excitability and conduction. A detailed analysis of the molecular mechanisms leading to the mutation-induced gain of expression and function was out of the scope of the present work. These findings, however, strongly support the role of TRPM4 gain-of-function in slowed cardiac impulse propagation.

5. Limitations

Next generation-based targeted resequencing such as HaloPlex™ System allows high-throughput genetic screening in a large number of individuals but some target sequences may be uncovered due to biases in DNA digestion by restriction enzymes. Thus some relevant variations may be missed in small subsets of coding regions: this problem is inherent to sequencing strategies based on DNA enrichment.

Furthermore this high-throughput candidate-gene approach was used to screen 19 candidate genes in 95 unrelated patients. Except for the patient carrying the *TRPM4*-p.I376T variant (patient 9) for which a familial recruitment, segregation tests and a LOD score calculation strongly suggest an association between this variant and the phenotype, the implication of variants in other unknown involved genes cannot be excluded in isolated PCCD cases.

6. Conclusion

In this study we identified one large family with 10 members diagnosed with PFHBI and carrying a *TRPM4* gain-of-expression and function mutation. This represents the first NGS-based detection of a *TRPM4* variant that has led to the recruitment of a large PCCD pedigree. This work confirms that gain-of-function mutations in the intracellular N-terminal region of TRPM4 are responsible for PFHBI and further underline the crucial role of TRPM4 channel in cardiac conduction disorders.

Supplementary data to this article can be found online at http://dx.doi.org/10.1016/j.ijcard.2016.01.052.

Authors' contributions

XD, MYA, HA, RR and JJS conceived the study, wrote the manuscript and are the guarantors of the project; PL, EC, JB and SLS contributed to the data processing; SB and EB performed the sequencing; BB and SN contributed to the functional and biochemical analyses; SF, AT and FK recruited the patients; HLM, NM, JBG and VP provided expert clinical advice; CD led the statistical analysis. All authors interpreted the data, contributed and commented on drafts of the article, and approved the final version.

Fundings

This work was supported by the Fondation pour la Recherche Médicale (FRM grant DEQ20140329545) to Jean-Jacques Schott; by the Institut National de la Santé et de la Recherche Médicale (INSERM, ATIP-Avenir program), the ANR-14-CE10-0001-01 (GenSuD) and the French Regional Council of Pays-de-la-Loire to Richard Redon; by the Centre National de la Recherche et de la Santé (CNRS grant – PRC CNRS/JSPS) to Jean-Jacques Schott and Naomasa Makita; by the French Ministry of Health (grant from the Clinical Research Hospital Program PHRC-I PROG11/33 in 2011) and the Fédération Française de Cardiologie (grant no. RC13_0012 in 2012) to Vincent Probst; and by the Swiss National Science Foundation to Hugues Abriel (310030B_14706035693), and the TransCure NCCR network, the Berne University Research Foundation.

Conflict of interest

The authors declare no conflict of interest.

Acknowledgments

We would like to thank the French clinical network against inherited cardiac arrhythmias as well as the patients who participated to this study for participation. We are also grateful to the members of the Genomics and Bioinformatics Core Facility of Nantes (Biogenouest) for their technical expertise.

References

[1] J. Lenègre, Etiology and pathology of bilateral bundle branch block in relation to complete heart block, Prog. Cardiovasc. Dis. 6 (1964) 409–444, http://dx.doi.org/10.1016/S0033-0620(64)80001-3.
[2] M. Lev, The pathology of complete atrioventricular block, Prog. Cardiovasc. Dis. 6 (1964) 317–326, http://dx.doi.org/10.1016/S0033-0620(64)80005-0.
[3] J.-J. Schott, D.W. Benson, C.T. Basson, et al., Congenital heart disease caused by mutations in the transcription factor NKX2-5, Science 281 (1998) 108–111, http://dx.doi.org/10.1126/science.281.5373.108.
[4] V. Probst, F. Kyndt, F. Potet, et al., Haploinsufficiency in combination with aging causes SCN5A-linked hereditary Lenègre disease, J. Am. Coll. Cardiol. 41 (2003) 643–652, http://dx.doi.org/10.1016/S0735-1097(02)02864-4.
[5] H. Watanabe, T.T. Koopmann, S. Le Scouarnec, et al., Sodium channel β1 subunit mutations associated with Brugada syndrome and cardiac conduction disease in humans, J. Clin. Invest. (2008)http://dx.doi.org/10.1172/JCI33891.
[6] M. Kruse, E. Schulze-Bahr, V. Corfield, et al., Impaired endocytosis of the ion channel TRPM4 is associated with human progressive familial heart block type I, J. Clin. Invest. 119 (2009) 2737–2744, http://dx.doi.org/10.1172/JCI38292.
[7] H. Liu, L.E. Zein, M. Kruse, et al., Gain-of-function mutations in TRPM4 cause autosomal dominant isolated cardiac conduction disease, Circ. Cardiovasc. Genet. 3 (2010) 374–385, http://dx.doi.org/10.1161/CIRCGENETICS.109.930867.
[8] D. Fatkin, C. MacRae, T. Sasaki, et al., Missense mutations in the rod domain of the lamin A/C gene as causes of dilated cardiomyopathy and conduction-system disease, N. Engl. J. Med. 341 (1999) 1715–1724, http://dx.doi.org/10.1056/NEJM199912023412302.
[9] C.-C. Lai, Y.-H. Yeh, W.-P. Hsieh, et al., Whole-exome sequencing to identify a novel LMNA gene mutation associated with inherited cardiac conduction disease, PLoS One 8 (2013)http://dx.doi.org/10.1371/journal.pone.0083322.
[10] N. Makita, A. Seki, N. Sumitomo, et al., A Connexin40 mutation associated with a malignant variant of progressive familial heart block type I, Circ. Arrhythm. Electrophysiol. 5 (2012) 163–172, http://dx.doi.org/10.1161/CIRCEP.111.967604.
[11] J.M. Combrink, W.H. Davis, H.W. Snyman, Familial bundle branch block, Am. Heart J. 64 (1962) 397–400, http://dx.doi.org/10.1016/0002-8703(62)90156-4.
[12] A.J. Brink, M. Torrington, Progressive familial heart block–two types, S. Afr. Med. J. 52 (1977) 53–59.

[13] E. Stéphan, Hereditary bundle branch system defect: survey of a family with four affected generations, Am. Heart J. 95 (1978) 89–95, http://dx.doi.org/10.1016/0002-8703(78)90401-5.
[14] M. Kruse, O. Pongs, TRPM4 channels in the cardiovascular system, Curr. Opin. Pharmacol. 15 (2014) 68–73, http://dx.doi.org/10.1016/j.coph.2013.12.003.
[15] H. Liu, S. Chatel, C. Simard, et al., Molecular genetics and functional anomalies in a series of 248 brugada cases with 11 mutations in the TRPM4 channel, PLoS One 8 (2013)http://dx.doi.org/10.1371/journal.pone.0054131.
[16] B. Stallmeyer, S. Zumhagen, I. Denjoy, et al., Mutational spectrum in the Ca2 + − activated cation channel gene TRPM4 in patients with cardiac conductance disturbances, Hum. Mutat. 33 (2012) 109–117, http://dx.doi.org/10.1002/humu.21599.
[17] S. B, C. R, D. BJ, G. LS, AHA/ACCF/HRS Recommendations for the Standardization and Interpretation of the Electrocardiogram Part III: Intraventricular Conduction Disturbances: A Scientific Statement From the American Heart Association Electrocardiography and Arrhythmias Committee, Council on Clinical Cardiology; the American College of Cardiology Foundation; and the Heart Rhythm Society: Endorsed by the International Society for Computerized Electrocardiology, Circulation 119 (2009) e235–e240, http://dx.doi.org/10.1161/CIRCULATIONAHA.108.191095.
[18] M.V. Elizari, R.S. Acunzo, M. Ferreiro, Hemiblocks revisited, Circulation 115 (2007) 1154–1163, http://dx.doi.org/10.1161/CIRCULATIONAHA.106.637389.
[19] S.L. Scouarnec, M. Karakachoff, J.-B. Gourraud, et al., Testing the burden of rare variation in arrhythmia-susceptibility genes provides new insights into molecular diagnosis for Brugada syndrome, Hum. Mol. Genet. (2015) ddv036, http://dx.doi.org/10.1093/hmg/ddv036.
[20] P. Kumar, S. Henikoff, P.C. Ng, Predicting the effects of coding non-synonymous variants on protein function using the SIFT algorithm, Nat. Protoc. 4 (2009) 1073–1081, http://dx.doi.org/10.1038/nprot.2009.86.
[21] I.A. Adzhubei, S. Schmidt, L. Peshkin, et al., A method and server for predicting damaging missense mutations, Nat. Methods 7 (2010) 248–249, http://dx.doi.org/10.1038/nmeth0410-248.
[22] P. Lindenbaum, S.L. Scouarnec, V. Portero, R. Redon, Knime4Bio: a set of custom nodes for the interpretation of next-generation sequencing data with KNIME, Bioinformatics 27 (2011) 3200–3201, http://dx.doi.org/10.1093/bioinformatics/btr554.
[23] N.E. Morton, Sequential tests for the detection of linkage, Am. J. Hum. Genet. 7 (1955) 277–318.
[24] M. Fishelson, D. Geiger, Exact genetic linkage computations for general pedigrees, Bioinformatics 18 (2002) S189–S198, http://dx.doi.org/10.1093/bioinformatics/18.suppl_1.S189.
[25] J.B. Gourraud, F. Kyndt, S. Fouchard, et al., Identification of a strong genetic background for progressive cardiac conduction defect by epidemiological approach, Heart 98 (2012) 1305–1310, http://dx.doi.org/10.1136/heartjnl-2012-301872.
[26] E.V. Davydov, D.L. Goode, M. Sirota, G.M. Cooper, A. Sidow, S. Batzoglou, Identifying a high fraction of the human genome to be under selective constraint using GERP++, PLoS Comput. Biol. 6 (2010) e1001025, http://dx.doi.org/10.1371/journal.pcbi.1001025.
[27] N. Syam, J.-S. Rougier, H. Abriel, Glycosylation of TRPM4 and TRPM5 channels: molecular determinants and functional aspects, Front. Cell. Neurosci. 8 (2014) 52, http://dx.doi.org/10.3389/fncel.2014.00052.
[28] M.-Y. Amarouch, N. Syam, H. Abriel, Biochemical, single-channel, whole-cell patch clamp, and pharmacological analyses of endogenous TRPM4 channels in HEK293 cells, Neurosci. Lett. 541 (2013) 105–110, http://dx.doi.org/10.1016/j.neulet.2013.02.011.
[29] H. Abriel, N. Syam, V. Sottas, M.Y. Amarouch, J.-S. Rougier, TRPM4 channels in the cardiovascular system: physiology, pathophysiology, and pharmacology, Biochem. Pharmacol. 84 (2012) 873–881, http://dx.doi.org/10.1016/j.bcp.2012.06.021.

JACC Vol. 24, No. 4
October 1994:1124–32

Distinct Gap Junction Protein Phenotypes in Cardiac Tissues With Disparate Conduction Properties

LLOYD M. DAVIS, MBBS, PHD, FRACP, H. LEE KANTER, MD, ERIC C. BEYER, MD, PHD, JEFFREY E. SAFFITZ, MD, PHD, FACC

Saint Louis, Missouri

Objectives. **We sought to characterize the connexin phenotypes of selected regions of the canine heart with different conduction properties to determine whether variations in connexin expression might contribute to the differences in intercellular resistance and conduction velocity that occur in different cardiac tissues.**

Background. **Gap junctions connect cardiac myocytes, allowing propagation of action potentials. Intercellular channels with different electrophysiologic properties are formed by different connexin proteins.**

Methods. **To determine which connexins were likely to be expressed in the sinus node, atrioventricular (AV) node and atrial and ventricular myocardium, messenger ribonucleic acids (RNAs) from each of these sites were hybridized with probes for connexin26, connexin31, connexin32, connexin37, connexin40, connexin43, connexin45, connexin46 and connexin50. Immunostaining with monospecific antibodies to connexin40, connexin43 and connexin45 was used to delineate the distribution of connexins in frozen sections of these different cardiac tissues.**

Results. **Only messenger RNAs coding for connexin40, connexin43 and connexin45 were detected by Northern blot analysis. By immunohistochemical staining, junctions in the sinus and AV nodes and proximal His bundle were virtually devoid of connexin43 but contained both connexin40 and connexin45. Gap junctions in the distal His bundle and the proximal bundle branches stained intensely for connexin40 and connexin43 and to a lesser extent for connexin45. Atrial gap junctions showed abundant staining of connexin43, connexin40 and connexin45. Ventricular gap junctions were characterized by abundant staining of connexin43 and connexin45 and much less staining of connexin40.**

Conclusions. **Although most cardiac gap junctions contain connexin40, connexin43 and connexin45, the relative amounts of each of these connexins vary considerably in cardiac tissues with different conduction properties.**

(J Am Coll Cardiol 1994;24:1124–32)

Gap junctions are specialized membrane structures containing multiple intercellular channels that permit the passage of ions and small molecules between cells. In the heart, they connect cardiac myocytes and are essential for rapid propagation of action potentials (1).

Intercellular channels in gap junctions are formed by proteins called connexins. At least 12 different connexins have been identified in mammals (2). Several of these have been shown to form channels with unique conductance and voltage dependence properties (3). Cardiac gap junctions contain several different connexins (4,5). The relative amounts and types of connexins appear to be different in cardiac tissues with different electrophysiologic properties. For example, we (5,6) have shown previously in the canine heart that connexin40 messenger ribonucleic acid (RNA) is three to five times more abundant in rapidly conducting Purkinje fibers than in more slowly conducting ventricular myocardium in which connexin43 is predominant. The composition of gap junctions in other areas of the heart with different electrophysiologic properties is not known. Immunostaining of connexin43 has been attempted in rabbit, rat and bovine nodal tissues with conflicting results. Connexin43 has been identified in the rabbit sinus nodes (7) but not in human or bovine sinus and atrioventricular (AV) nodes (8,9). Some investigators (10) have identified connexin43 in the rat sinus node, whereas others (11) have not detected connexin43 in these tissues. It has not been determined whether connexins other than connexin43 are present in these cardiac tissues.

Because different connexins form channels with different conductance and voltage dependence properties and connexin phenotypes differ in some tissues with different electrophysiologic properties, we hypothesized that variations in the number, size and connexin composition of gap junctions should result in changes in intercellular resistance to current flow and, hence, may be a major mechanism for regulating conduction

From the Departments of Pediatrics, Medicine, Cell Biology and Pathology, Washington University School of Medicine, Saint Louis, Missouri. This work was supported by Grants HL45466 and HL17646, SCOR in Coronary and Vascular Diseases, National Heart, Lung, and Blood Institute, National Institutes of Health, Bethesda, Maryland. Dr. Davis was supported by the B.J. Amos Award from the Westmead Medical Association, Sydney, Australia. Dr. Kanter was supported by a fellowship from the North American Society of Pacing and Electrophysiology, Newton Upper Falls, Massachusetts. Dr. Beyer was supported by an Established Investigator Award from the American Heart Association, Dallas, Texas.

Manuscript received January 21, 1994; revised manuscript received April 5, 1994, accepted May 10, 1994.

Address for correspondence: Dr. Jeffrey E. Saffitz, Department of Pathology, Box 8118, Washington University School of Medicine, 660 South Euclid Avenue, Saint Louis, Missouri 63110.

0735-1097/94/$7.00

velocity and the pattern of activation of normal and diseased cardiac tissue. As a first step in examining this hypothesis, we compared the protein composition of gap junctions in the canine sinus and AV nodes, in which conduction is slow, with that in the right atrium, the bundle of His and proximal bundle branches and ventricular myocardium, all of which conduct more rapidly.

Methods

Tissue acquisition. The sinus and AV node regions were dissected from the hearts of eight adult mongrel dogs under deep anesthesia induced with sodium pentothal. For immunostaining experiments the sinus node was dissected in a tissue block that contained the adjacent right atrium. For Northern blot analyses, the sinus node was dissected as cleanly as possible from the adjacent atrial muscle. The sinus node could be seen grossly on the epicardial surface as a grayish strip of tissue ~2 mm in width and 10 to 15 mm in length surrounding the sinus node artery and adjacent to the atrial muscle of the crista terminalis. This strip of tissue was dissected and used to prepare RNA from the sinus node region. This sample contained the entire sinus node as well as some adjacent atrial myocytes and vascular smooth muscle and endothelium, neural tissue and fibrous connective tissue. The atrial muscle that remained after the sinus node region had been removed was also used for preparation of RNA for Northern blot analysis.

The AV node samples used for preparation of total RNA included all tissues within the posterior interatrial space. These tissue samples were bounded superiorly by the tendon of Todaro, inferiorly by the tricuspid and mitral valve annuli, posteriorly by the coronary sinus and anteriorly by the central fibrous body. Thus, these samples presumably included the entire AV node and most of the His bundle as well as contaminating myocardium and nonmyocytic cells from this region. The entire tissue block from the posterior interatrial space from eight canine hearts was used for RNA preparation and immunohistochemical studies.

The protocol used in these studies was approved by the Washington University Animal Studies Committee. All dogs received humane care in accordance with the requirements of the National Academy of Science and National Institutes of Health (NIH publication no. 86-23, revised 1985).

Northern blot analyses. To determine which of the known mammalian connexins are expressed in different cardiac tissues, total cellular RNA was prepared from the sinus node region, right atrial myocardium, AV node (triangle of Koch) and the interventricular septum from two adult dog hearts using the guanidinium isothiocyanate method of Chomczynski and Sacchi (12). Ribonucleic acid samples were electrophoresed through formaldehyde-agarose gels and transferred to nylon membranes as described previously (4). Each lane was loaded with 10 μg of RNA except for the membrane probed with connexin45 in which each lane contained 40 μg of RNA. The amount of RNA transferred onto each lane of the nylon membranes was determined by visual assessment under ultraviolet light of gels and membranes stained with ethidium bromide and by subsequent hybridization of membranes with a probe for 18S ribosomal RNA. Within each Northern blot experiment, approximately similar amounts of RNA were loaded and transferred as judged by the preceding criteria.

Membranes containing RNA from the sinus node region, AV node region, right atrium and ventricular septum were hybridized with phosphorus-32–labeled deoxyribonucleic acid (DNA) probes corresponding to bases 1 to 681 of rat connexin26 DNA (13), bases 1 to 813 of rat connexin31 DNA (14), bases 1 to 1,494 of rat connexin32 DNA (15), bases 1 to 1,601 of human connexin37 DNA, (16), bases 667 to 1,391 of dog connexin40 DNA (4), bases 1 to 1,393 of rat connexin43 DNA (17), bases 408 to 1,191 of dog connexin45 DNA (4), bases 1 to 1,592 of rat connexin46 DNA (18) and bases 267 to 1,589 of mouse connexin50 DNA (19). Probes were labeled with phosphorus-32 using random hexanucleotide primers and the Klenow fragment of DNA polymerase 1. Standard hybridization conditions with stringent washes were used for all blots (4). Positive Northern blot analyses were confirmed in two additional experiments by repeated hybridization of the same DNA probes with RNAs isolated from tissues of two other canine hearts.

Anticonnexin antibodies. Connexin43 was detected with a mouse monoclonal immunoglobulin G (IgG) antibody raised against amino acids 252 to 270 of rat connexin43 (Chemicon International Inc). Connexin40 was detected using affinity-purified polyclonal rabbit antibodies raised against residues 316 to 329 of dog connexin40. Connexin45 was detected using affinity-purified rabbit polyclonal antibodies raised against residues 285 to 298 of dog connexin45. We (4,5,20) have previously described the preparation and characterization of these monospecific antibodies. In brief, their specificity and absence of cross-reactivity were demonstrated by inhibition of immunostaining by coincubation of antibodies with their corresponding peptide immunogens, by immunoprecipitation experiments in which the connexin40 and connexin45 antibodies (and a connexin43 polyclonal antiserum that was raised against a peptide of 20 amino acids, including the 19 used for the connexin43 monoclonal antibody) precipitated only the relevant connexin, and confirmation by electron microscopy that these antibodies bind only to gap junctions rather than to other membrane structures (4,5,20).

Tissue preparation and immunohistochemical staining technique. Freshly dissected tissue was frozen immediately in liquid nitrogen. In three dog hearts, the sinus node with the adjacent right atrium and the AV node in the surrounding triangle of Koch were cut into 12-μm thick frozen sections. In three additional hearts frozen sections were prepared from regions containing the proximal left and right bundle branches and distal His bundle. Sections were cut in a plane parallel to the long axes of the cells of interest and mounted on gelatin-coated slides.

Sections were washed in phosphate-buffered saline solution and then preincubated for 30 min in blocking buffer composed of 3% normal goat serum, 0.4% nonfat dry milk, 2% IgG-free bovine serum albumin (Sigma Chemical) and 0.3% Triton X-100 in phosphate-buffered saline solution. Sections were

incubated overnight with the respective primary antibody diluted 1:400 in blocking buffer. For double-labeling studies, sections were incubated overnight with a combination of antibodies against connexin43 and either connexin40 or connexin45 in the preceding blocking buffer. Nonimmune mouse serum, nonimmune rabbit serum and a mixture of both sera were used as negative controls. After washing in phosphate-buffered saline solution, the single-label sections were incubated with a 1:800 dilution of the appropriate rabbit or mouse secondary antibody conjugated to CY3 (Jackson Immunoresearch Laboratories). For double-label studies, sections were coincubated with a 1:800 dilution of CY3-labeled anti-rabbit IgG and a 1:200 dilution of fluorescein isothiocyanate-labeled anti-mouse IgG (Boehringer Mannheim). Double- and single-labeled sections were examined by conventional fluorescence microscopy with filter sets appropriate for the specific fluorochromes.

Results

Northern blot analyses. Multiple Northern blots of RNA prepared from the canine sinus node, right atrium, triangle of Koch (containing the AV node) and the interventricular septum were hybridized with phosphorus-32 DNA probes that specifically recognized messenger RNAs of connexin phenotypes 26, 31, 32, 37, 40, 43, 45, 46 and 50. Bands corresponding to connexin43, connexin40 and connexin45 messenger RNAs were detected in all tissues (Fig. 1), indicating that messenger RNAs for these connexins were present in some or all of the cells in each of these regions. Although precise quantification of the relative amounts of messenger RNA in different cardiac tissues cannot be made because of the inability to cleanly dissect out nodal tissue from surrounding atrial and ventricular tissues, some differences were apparent. The probe for connexin40 hybridized with three bands (4.5, 3.3 and 2.5 kilobases [kb]) in nodal tissues and two bands (4.5 and 2.5 kb) in atrial and ventricular muscle. Multiple connexin40 messenger RNAs have also been observed in previous studies of dog myocardium (4). Messenger RNAs for all the other tested connexins (connexin phenotypes 26, 31, 32, 37, 46 and 50) were not detected in any tissues. Therefore, subsequent immunohistochemical experiments were limited to examining expression of only connexin 40, 43 and 45.

Immunohistochemistry. The results of immunostaining experiments are summarized in Table 1. Intercellular sites were judged visually to have abundant, moderate, scant or absent immunostaining with antibodies to connexin40, connexin43 and connexin45. Similarly, the sizes of gap junctions were determined visually to be large, moderate or small. The numbers of gap junctions were scored as many, moderate and few.

Conduction system. The sinus and AV nodes had the same pattern of immunostaining (Fig. 2 and 3). Small, sparse areas of immunofluorescence were observed with antibodies to connexin40 and connexin45 in a distribution consistent with the known distribution of small gap junctions in these tissues. No connexin43 immunostaining was observed in either the

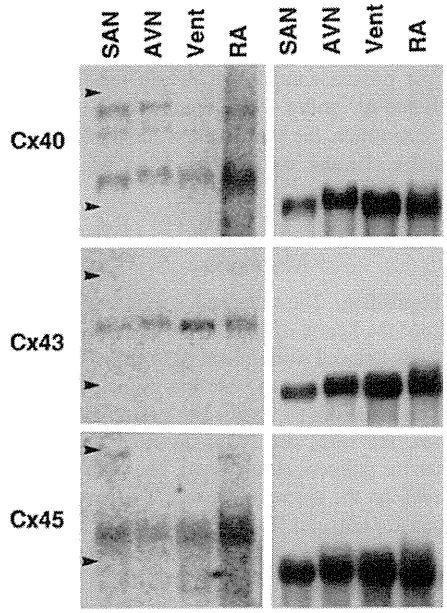

Figure 1. Northern blots of connexin (Cx) messenger ribonucleic acids (RNAs) in canine sinoatrial node region (SAN), atrioventricular node region (AVN), interventricular septum (Vent) and right atrium (RA). Autoradiographs were developed after a 6-day exposure for connexin40, an overnight film exposure for connexin43 and a 3-day film exposure for connexin45. For the connexin40 and connexin43 hybridizations, 10 μg of RNA was loaded in each lane; for the connexin45 experiment, 40 μg of RNA was loaded in each lane. The **right panels** show the results of hybridizing the same membranes with a probe for 18S ribosomal RNA.

Table 1. Characteristics of Canine Cardiac Gap Junctions Determined by Immunohistochemistry

Cardiac Tissue	Gap Junction Structure		Connexin Phenotype		
	Size	Number	40	43	45
Sinus node	Small	Few	Scant	Absent	Scant
Atrioventricular node and proximal His bundle	Small	Few	Scant	Absent	Scant
Distal His bundle and proximal bundle branches	Large	Moderate	Abundant	Abundant	Moderate
Right atrium	Large	Many	Abundant	Abundant	Moderate
Ventricle	Moderate	Many	Scant	Abundant	Moderate

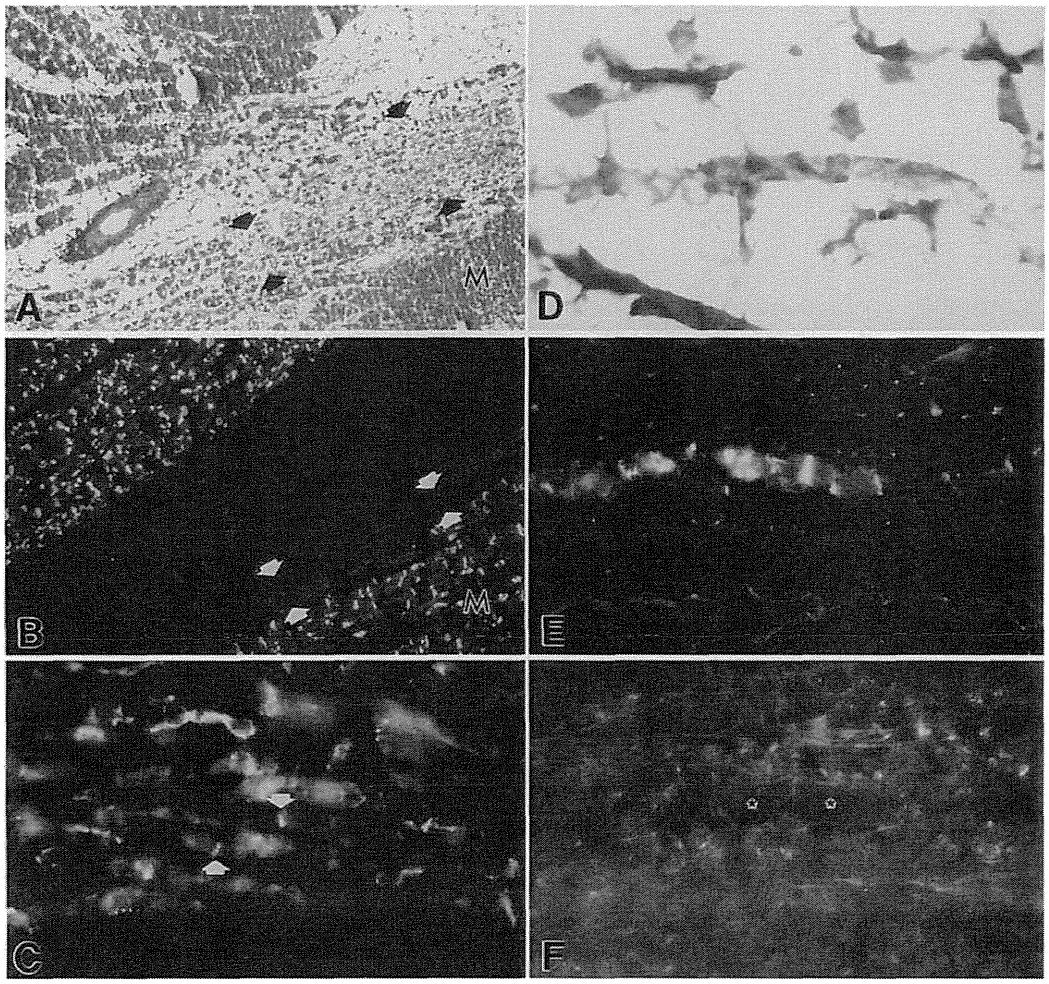

Figure 2. Immunohistochemical delineation of connexin expression in the canine sinus node. **A,** Low power view of the sinoatrial node region stained with Masson's trichrome. The sinoatrial node artery is surrounded by nodal myocytes (**arrows**) and connective tissue. Atrial myocardium (M) is present at the edges of the section. **B,** Low power view of an adjacent section of the sinoatrial node region to **A** stained with anticonnexin43 antibodies. Junctions in atrial muscle (M) above and below the node region are prominently stained. The large unstained region in the **center** of the panel includes the sinoatrial node artery, adjacent sinoatrial node myocytes and intervening perivascular connective tissue. A group of sinoatrial node myocytes, located **between the arrows**, exhibits no connexin43 immunoreactivity. **C,** High power view of sinoatrial node cells stained with antibodies against connexin45. Multiple areas of intense fluorescent signal are seen at points of apparent contact between cells (some shown by **arrows**). The less intense fluorescence in other areas of the tissue is due in part to staining of junctional material out of the plane of focus in this high power micrograph of a 12-μm thick section. **D,** High power view of part of the sinoatrial node stained with Masson's trichrome. A strand of sinoatrial node cells is present in the **center** of the image surrounded by abundant connective tissue. **E** and **F,** Double-labeled preparation of a strand of sinoatrial node cells adjacent to the node artery taken from an adjacent section to that shown in panel **D.** Junctions are clearly stained with antibodies against connexin40 (**E**) but when viewed under conditions to visualize connexin43 immunoreactivity (**F**), only background level signal is seen. The **unstained regions** above and below the strand of sinoatrial node myocytes shown in **D** and corresponding to the regions of low intensity fluorescence in **E** contain adjacent connective tissue. The connexin43-stained preparation (**E**) was deliberately overexposed to document the absence of connexin43 immunoreactivity in the sinoatrial node myocytes. The region occupied by the node cells (**asterisks**) shows no staining. Original magnification ×80 (**A**), ×100 (**B**), ×500 (**C** to **F**); all reduced by 25%.

sinus or the AV node. Connexin43 was detected in only a few isolated atrial myocytes in the sinus node and some atrial myocytes that infiltrated the edges of the AV node. Thus, the relatively weak connexin43 signals observed in Northern blots of RNA extracted from the sinoatrial and AV node regions were undoubtedly attributable to nonnodal cells unavoidably included in these samples. The gap junctions in the sinus and

JACC Vol. 24, No. 4
October 1994:1124–32

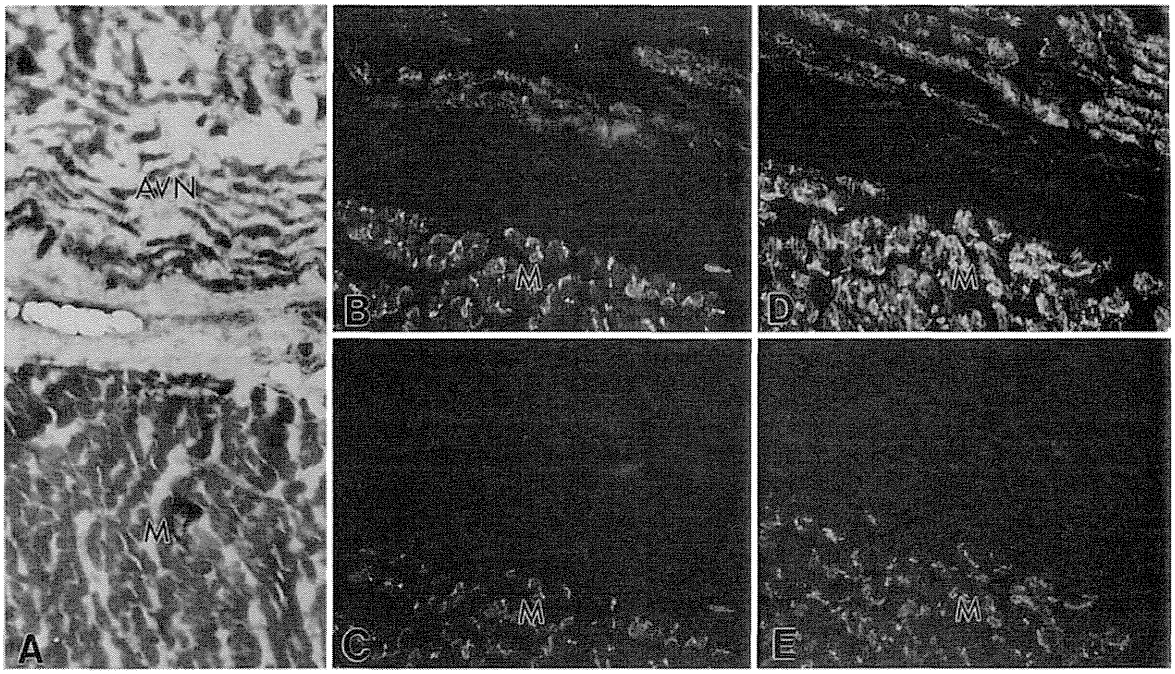

AV nodes were smaller and stained less intensely for connexins than those in the surrounding atrial and ventricular tissue.

In the proximal bundle of His, as in the nodal tissues, intercellular areas of immunostaining also were small and reacted specifically with antibodies to connexin40 and connexin45 but weakly or not at all to connexin43. The pattern of immunostaining and the size of the gap junctions changed in the distal His bundle to become the same as those in the bundle branches (Fig. 4). These gap junctions were large and stained intensely with antibodies to connexin40 and connexin43 and to a lesser degree connexin45.

Atrial and ventricular myocardium. Antibodies to connexin43, connexin40 and connexin45 bound to intercellular membranes in a pattern consistent with the distribution of gap junctions between right atrial myocytes and between ventricular myocytes (Fig. 4 and 5). Connexin40 staining was prominent in right atrial gap junctions but considerably less intense in ventricular muscle junctions. There was no apparent difference in the intensity of connexin43 or connexin45 staining in ventricular and atrial muscle gap junctions.

Figure 3. Atrioventricular (AV) node. **A,** Section of the AV node region stained with Masson's trichrome. The small nodal cells (AVN) are separated from the adjacent ventricular myocardium (M) by the tricuspid annulus. **B** and **C,** Section of the AV node region adjacent to **A** double-labeled with antibodies against connexin40 (**B**) and connexin43 (**C**). Both the nodal cells and the adjacent myocardium (M) stain with anticonnexin40 antibodies, but connexin43 staining is seen only in the adjacent myocardium. **D** and **E,** Section of AV node region stained with anticonnexin45 (**D**) and anticonnexin43 (**E**) antibodies. Junctions in both the node and the adjacent myocardium show connexin45 immunoreactivity, but only the myocardium stains for connexin43. The **unstained regions** seen in the **center** of **B** and **D** represent collagenous connective tissue separating nodal tissue from the adjacent myocardium. Original magnification ×150 (**A**), ×100 (**B** to **D**); all reduced by 25%.

Discussion

The results of this study demonstrate that gap junctions in the canine sinus and AV nodes and the proximal bundle of His contain connexin40 and connexin45 but not connexin43. These are the only known cardiac tissues that lack connexin43. In contrast to the nodal tissues, most gap junctions in other cardiac tissues contain connexin40, connexin43 and connexin45. However, the relative amounts of these connexins vary considerably in different areas of the heart with different conduction properties.

We have found no previous studies that delineate the multiple connexin phenotypes of the mammalian cardiac conduction system and myocardium. However, some data (6–11,15–17,26–29) have been published on the presence of RNA coding for different connexins in the ventricles and on the distribution of connexin43 determined by immunostaining in some parts of the heart. Most of these studies are supportive of our findings.

Connexin messenger RNA in cardiac tissues. In the current study, only messenger RNAs coding for connexin40, connexin43 and connexin45 were detected. All these messenger RNAs were present in each of the examined tissues. However samples from nodal tissues were clearly contaminated by adjacent nonnodal myocardium, preventing any direct

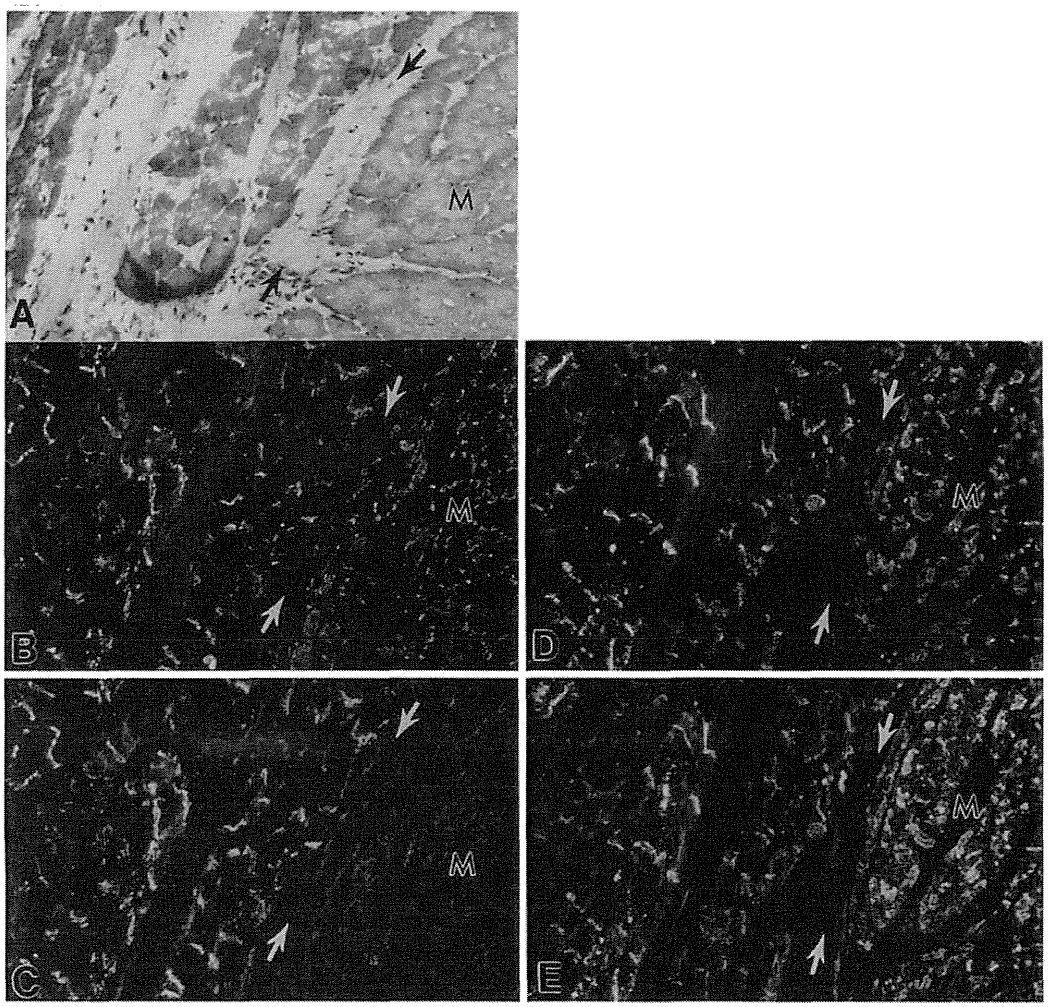

Figure 4. Immunohistochemical delineation of connexin expression in the proximal bundle branches. **A,** Section of the proximal left bundle and adjacent crest of the ventricular septum (M) stained with Masson's trichrome. **B** and **C,** Adjacent section to **A** near the crest of the ventricular septum including the proximal left bundle and adjacent ventricular muscle (M) double-labeled with anticonnexin43 and anticonnexin40 antibodies. The location of the connective tissue septum separating the conduction bundle from the ventricular muscle is indicated by the **arrows**. The large junctions of the bundle stain prominently for both connexin43 **(B)** and connexin40 **(C)**. In contrast, the ventricular muscle exhibits abundant connexin43 immunoreactivity **(B)** but much less apparent connexin40 staining **(C)**. **D** and **E,** Section of the proximal left bundle and adjacent ventricular muscle (M) double-labeled with connexin43 and connexin45 antibodies. The fibrous tissue between the bundle and the ventricular muscle is shown by **arrows**. Both the bundle and the ventricular muscle stain for connexin43 **(D)** and connexin45 **(E)**. Original magnification ×175 **(A** to **E)**; all reduced by 25%.

comparison of the relative amounts of messenger RNA and protein in these tissues. This same problem also probably explains why significant amounts of messenger RNA coding for connexin43 were detected in RNA derived from the nodal regions even though connexin43 protein could not be detected at these sites. These findings are in keeping with our previous findings (6,21) of mRNAs coding for connexin40, connexin43 and connexin45 in canine and human left ventricles. Others have also reported the presence of RNA coding for connexin43 in rat, mouse and bovine ventricles but have not assayed for the presence of connexin40 and connexin45 (22,23). Although we surveyed the heart with probes for the majority of the known connexins, it is possible that low levels of some of these or of other so far undiscovered proteins that form intercellular channels also may contribute to intercellular conduction in the dog heart. Because some of the probes were produced from rodent, human or bovine DNA sequences, it is possible that the canine homologs went undetected. However, in view of the high degree of connexin sequence homology in mammals, this possibility seems unlikely. We (16) have previously detected low levels of RNA coding for connexin37 in mouse ventricle, and Paul (15) has reported the presence of small amounts of

JACC Vol. 24, No. 4
October 1994:1124–32

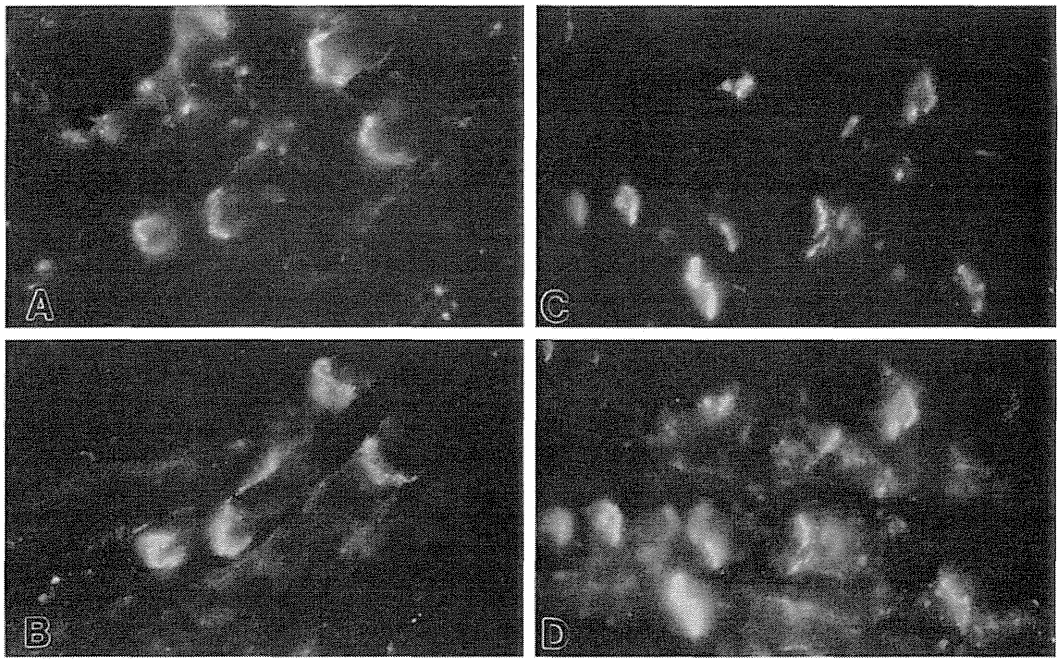

Figure 5. Sections of right atrium showing prominent staining of junctions in preparations double labeled with anticonnexin43 (**A**) and anticonnexin45 (**B**) antibodies and anticonnexin43 (**C**) and anticonnexin40 (**D**) antibodies. Original magnification ×500 (**A** to **D**); all reduced by 25%.

connexin46 messenger RNA in rat ventricle. Gourdie et al. (10) have detected material immunoreactive with an anti-MP70 antibody in rat cardiac valve tissues (although White et al. [19] did not detect messenger RNA for connexin50, which may encode MP70 in mouse heart). However, RNA coding for these connexins was not detected in any of the samples taken from the dog heart. In addition, we did not examine connexin30.3, connexin31.1 and connexin33. So far these connexins have been detected only in skin and testes (24,25).

The probe for connexin40 hybridized with multiple RNA bands, a result we have observed in previous studies (4). Because of the stringent hybridization conditions used, the multiple connexin40 bands are likely to be closely related messenger RNA species, perhaps alternately processed connexin40 messenger RNAs. However, multiple splice forms of messenger RNAs coding for connexin40 or any other connexin have not been described. Further studies will be required to determine whether this explanation is correct or whether the multiple bands represent cross-hybridization with RNAs of other closely related proteins.

Connexin phenotypes of gap junctions in the cardiac conduction system. Previous immunostaining studies have produced conflicting descriptions of the distribution connexin43 in the cardiac conduction system. As in our study in the canine heart, Van Kempen et al. (11) did not detect connexin43 in the gap junctions of the rat and mouse sinus and AV nodes. Oosthoek et al. (8,9) have made similar observations in the nodal tissues of human, rat and bovine hearts.

In contrast to these results, Gourdie et al. (10) and Anumonwo et al. (7) detected connexin43 in the rat AV node and the rabbit sinus node, respectively. Differences in antibody specificities and immunostaining methods may explain some of these conflicting results. The use of confocal microscopy by Gourdie et al. (10) may have enhanced detection of weakly staining gap junctions by reducing background artifact. However, we were unable to detect connexin43 in the nodal tissues even when the preparations were viewed with confocal microscopy. Interspecies variability in connexin expression may also account for the differences in staining patterns found between the rabbit and canine sinus nodes and may explain the absence of connexin43 in the rat His and proximal bundles reported by Gourdie et al. (10) and the presence of connexin43 in these tissues in the canine heart in our study.

Connexin phenotypes in the right atrium and ventricle. Our study demonstrates that canine right atrial gap junctions contain mainly connexin40 and connexin43 and a lesser amount of connexin45, whereas ventricular gap junctions are composed predominantly of connexin43 and connexin45. These results confirm our previous observations (6) about the composition of the gap junctions in the canine ventricle. In contrast to our results, Bruzzone et al. (26) did not detect connexin40 immunostaining in rat ventricular myocytes. These disparate results may be due to technical differences in tissue handling, the affinities and specificities of the different anti-

bodies for connexin40 and the reagents used for immunostaining. Further studies in which both connexin40 antibodies are compared in the same tissues may resolve this discrepancy.

There is little controversy about the presence of connexin43 in both atrial and ventricular gap junctions. Abundant connexin43 staining was shown in the rat heart by Van Kempen et al. (11), in ventricular gap junctions of the dog heart by Dolber et al. (27) and in ventricular junctions of the mouse heart by Yancey et al. (28). Peters et al. (29) observed abundant connexin43 staining in the human ventricle.

Functional implications. The biologic advantages of having multiple distinct connexin phenotypes in different parts of the heart and conduction system are not known. Although our data allow only qualitative comparisons with the functional data of others, some potential reasons for the diversity of connexin phenotypes in the heart are apparent. Because different connexins form channels with different conductances, voltage sensitivities and ion permeabilities, changes in the connexin phenotypes of tissue may influence intercellular resistance, conduction velocity and electrotonic interactions between cells (30). This concept is supported by the highly variable distribution of connexins in cardiac tissues having distinct electrophysiologic characteristics. Connexin40 forms channels with larger unitary conductances than connexin43 (3,31,32). Therefore, we had speculated previously that the expression of large amounts of connexin40 might contribute to the more rapid conduction in Purkinje fibers. However, our current data present the puzzling results that connexin40 is most abundant both in the most rapidly conducting and in slowly conducting regions of the heart (6).

Perhaps this apparent paradox is explained by differential regulation of connexin40 in different cardiac tissues. Although there are no data to prove this hypothesis about connexin40, Takens Kwak and Jongsma (33) recently demonstrated that phosphorylating treatments produced three different single-channel conductances in neonatal rat cardiac myocytes. Moreno et al. (34) suggested that differential phosphorylation produced different unitary conductances in connexin43 transfected cells. Furthermore, variations in connexin expression are not the only determinant of intercellular resistance. Intercellular resistance and conduction velocity are determined by the total number and type of connexins, the regulation of the opening and closing states of intercellular channels, the size and spatial arrangement of gap junctions between cells, the size and shape of adjoining cells as well as the active membrane properties of cells. Many of these structural and molecular features differ substantially in different parts of the cardiac conduction system. For example, gap junctions in the sinus node are smaller and occupy a smaller proportion of the cell membrane than do those in the surrounding atria (35,36). Anumonwo et al. (7) and Lorente et al. (37) have identified different membrane resistances of cells in the sinus nodes (1.1 GΩ) and ventricle (28 MΩ).

Differences in connexin phenotypes may also be important in differential regulation of intercellular exchange of small molecules that control differentiation. Although the ontogeny of the conduction system is incompletely understood, there is some evidence to suggest that nodal tissues and the proximal bundle branches arise from a common progenitor separate from that of the atria and ventricles (38). Accordingly, it is not surprising that nodal tissues have a unique connexin phenotype distinct from that of atrial and ventricular myocardium. Nevertheless, additional studies on the number, size and spatial arrangement of gap junctions in each area of the conduction system and on the effects of altering the connexin phenotypes on cardiac development and function will be required before definite conclusions on the functional significance of specific connexin phenotypes can be reached.

Conclusions. Most cardiac gap junctions are formed by connexin40, connexin43 and connexin45. The relative amounts of each of the these connexins vary in different cardiac regions with different conduction properties. In contrast to contractile myocardium, junctions in the canine sinus and AV nodes are formed by connexin40 and connexin45 and do not appear to contain connexin43.

We thank Dana Abendschein, PhD and Pam Lundius, LAT for supplying the canine tissue.

References

1. Barr L, Dewey MM, Berger W. Propagation of action potentials and the structure of the nexus in cardiac muscle. J Gen Physiol 1965;48:797–823.
2. Beyer E. Gap junctions. Int Rev Cytol 1993;137:1–37.
3. Veenstra RD, Wang HZ, Westphale EM, Beyer EC. Multiple connexins confer distinct regulatory and conductance properties of gap junctions in developing heart. Circ Res 1992;71:1277–83.
4. Kanter HL, Saffitz JE, Beyer EC. Cardiac myocytes express multiple gap junction proteins. Circ Res 1992;70:438–44.
5. Kanter HL, Laing JG, Beyer EC, Green KG, Saffitz JE. Multiple connexins colocalize in canine ventricular myocyte gap junctions. Circ Res 1993;73:344–50.
6. Kanter HL, Laing JG, Beau SL, Beyer EC, Saffitz JE. Distinct patterns of connexin expression in canine Purkinje fibers and ventricular muscle. Circ Res 1993;72:1124–31.
7. Anumonwo JMB, Wang H-Z, Trabka-Janik E, et al. Gap junctional channels in adult mammalian sinus nodal cells: immunolocalization and electrophysiology. Circ Res 1992;71:229–39.
8. Oosthoek PW, Viragh S, Lamers WH, Moorman AFM. Immunohistochemical delineation of the conduction system. II. The atrioventricular node and the Purkinje fibers. Circ Res 1993;73:482–91.
9. Oosthoek PW, Viragh S, Mayen AEM, Van Kempen MJA, Lamers WH, Moorman AFM. Immunohistochemical delineation of the conduction system. I. The sinoatrial node. Circ Res 1993;73:473–81.
10. Gourdie R, Green C, Severs N, Thompson R. Immunolabelling patterns of gap junction connexins in the developing and mature rat heart. Anat Embryol (Berl) 1992;185:363–78.
11. Van Kempen MJA, Fromaget C, Gros D, Moorman AFM, Lamers WH. Spatial distribution of connexin 43, the major cardiac gap junction protein, in the developing and adult rat heart. Circ Res 1991;68:1638–51.
12. Chomczynski P, Sacchi N. Single-step method of RNA isolation by acid guanidinium thiocyanate-phenol-chloroform extraction. Anal Biochem 1987;162:156–9.
13. Zhang J-T, Nicholson BJ. Sequence and tissue distribution of a second protein of hepatic gap junctions, connexin26, as deduced from its cDNA. J Cell Biol 1989;109:3391–401.
14. Hoh JH, John S, Revel J-P. Molecular cloning and characterization of a new member of the gap junction gene family, connexin-31. J Biol Chem 1991;266:6524–31.

15. Paul DL. Molecular cloning of cDNA for rat liver gap junction protein. J Cell Biol 1986;103:123–34.
16. Reed KE, Westphale EM, Larson DM, Wang HZ, Veenstra RD, Beyer EC. Molecular cloning and functional expression of human connexin 37, an endothelial cell gap junction protein. J Clin Invest 1993;91:997–1004.
17. Beyer EC, Paul DL, Goodenough DA. Connexin43: a protein from rat heart homologous to a gap junction in liver. J Cell Biol 1987;105:2621–9.
18. Paul DL, Ebihara L, Takemoto LJ, Swenson KI, Goodenough DA. Connexin46, a novel lens gap junction protein, induces voltage-gated currents in nonjunctional plasma membrane of *Xenopus* oocytes. J Cell Biol 1991;115: 1077–89.
19. White TW, Bruzzone R, Goodenough DA, Paul DL. Mouse connexin50, a functional member of the connexin family of gap junction proteins, is the lens fiber protein MP70. Mol Biol Cell 1992;3:711–20.
20. Beyer EC, Kistler J, Paul DL, Goodenough DA. Antisera directed against connexin43 peptides react with a 43-kD protein localized to gap junctions in myocardium and other tissues. J Cell Biol 1989;108:595–605.
21. Chen S-C, Westphale E, Beyer EC, Saffitz JE. Human fetal and infant hearts express multiple connexins [abstract]. Circulation 1993;88 Suppl I:I-437.
22. Fromaget C, El AA, Dupont E, Briand JP, Gros D. Changes in the expression of connexin 43, a cardiac gap junctional protein, during mouse heart development. J Mol Cell Cardiol 1990;22:1245–58.
23. Fishman GI, Hertzberg EL, Spray DC, Leinwand LA. Expression of connexin 43 in the developing rat heart. Circ Res 1991;68:782–7.
24. Hennemann H, Dahl E, White JB, et al. Two gap junction genes, connexin *31.1 and 30.3* are closely linked on mouse chromosome 4 and preferentially expressed in skin. J Biol Chem 1992;267:17225–33.
25. Haefliger JA, Bruzzone R, Jenkins NA, Gilbert DJ, Copeland NG, Paul DL. Four novel members of the connexin family of gap junction proteins. Molecular cloning, expression and chromosome mapping. J Biol Chem 1992;267:2057–64.
26. Bruzzone R, Haefliger JA, Gimlich RL, Paul DL. Connexin40, a component of gap junctions in vascular endothelium, is restricted in its ability to interact with other connexins. Mol Biol Cell 1993;4:7–20.
27. Dolber PC, Beyer EC, Junker JL, Spach MS. Distribution of gap junctions in dog and rat ventricle studied with a double-label technique. J Mol Cell Cardiol 1992;24:1443–57.
28. Yancey SB, Biswal S, Revel JP. Spatial and temporal patterns of distribution of the gap junction protein connexin43 during mouse gastrulation and organogenesis. Development (Camb) 1992;114:203–12.
29. Peters NS, Green CR, Poole-Wilson PA, Severs NJ. Reduced content of connexin43 gap junctions in ventricular myocardium from hypertrophied and ischaemic human hearts. Circulation 1993;88:864–75.
30. Cranefield PF. The conduction of the cardiac impulse, 1951–1986. Experientia 1987;43:1040–4.
31. Fishman GI, Spray DC, Leinwand LA. Molecular characterization and functional expression of the human cardiac gap junction channel. J Cell Biol 1990;111:589–98.
32. Veenstra RD, Beblo DA, Wang H-Z, Westphale EM, Beyer EC. Unique ionic conductance and selectivity of connexin40 channels, a major gap junction protein in conducting tissues [abstract]. Circulation 1993;88 Suppl I:I-175.
33. Takens Kwak BR, Jongsma HJ. Cardiac gap junctions: three distinct single channel conductances and the modulation by phosphorylating treatments. Pflugers Arch 1992;422:198–200.
34. Moreno AP, Fishman GI, Spray DC. Phosphorylation shifts unitary conductance and modities voltage dependent kinetics of human connexin43 gap junction channels. Biophys J 1992;62:51–3.
35. Masson-Pevet M, Bleeker WK, Gros D. The plasma membrane of leading pacemaker cells in the rabbit sinus node: a qualitative and quantitative ultrastructural analysis. Circ Res 1979;45:621–9.
36. Page E, Shibata Y. Permeable junctions between cardiac cells. Annu Rev Physiol 1981;43:431–41.
37. Lorente P, Delgado C, Delmar M, Henzel D, Jalife J. Hysteresis in the excitability of isolated guinea pig ventricular myocytes. Circ Res 1991;69: 1301–5.
38. Ikeda T, Iwasaki K, Shimokawa I, Sakai H, Ito H, Matsuo T. Leu-7 immunoreactivity in human and rat embryonic hearts, with special reference to the development of the conduction tissue. Anat Embryol (Berl) 1990;182: 553–62.

Advance Publication by-J-STAGE

Circulation Journal
Official Journal of the Japanese Circulation Society
http://www.j-circ.or.jp

EDITORIAL

E1784K Mutation in *SCN5A* and Overlap Syndrome

Naokata Sumitomo, MD, PhD

Congenital long QT syndrome (LQTS) is characterized by prolongation of the QT interval on the surface ECG and may cause syncope and seizures; there is a certain risk of fatal ventricular arrhythmias, torsade de pointes or ventricular fibrillation.[1] The QT interval is determined by the cardiac action potential duration and is related to the many ion channels in the myocardial cells. The most important state of the ion currents for prolonging the QT interval is a decrease in the outward K current, and increase of the inward Na or Ca current. *SCN5A* is the gene encoding the most prevalent cardiac Na channel α subunit, and an *SCN5A* mutation is responsible for many hereditary arrhythmias including type 3 LQTS (LQT3),[2] Brugada syndrome (BrS),[3] progressive cardiac conduction disturbances (PCCD),[4] sick sinus syndrome (SSS),[5,6] atrial fibrillation,[6,7] atrial standstill, and sudden infant death syndrome (SIDS).[8–10]

Article p????

The most common *SCN5A* mutation in LQT3 causes a persistent Na current during the action potential plateau because of malfunctioning of the fast Na channel inactivation,[2] and this delayed inactivation delays the repolarization of the myocardial cells, and leads to prolongation of the QT interval (**Table**).

In contrast, a reduction in the initial opening of the Na channels in the right ventricular epicardial cells may cause ST elevation in the right precordial leads and lead to BrS (**Table**).

Some PCCD patients develop this phenotype with aging, because the increased chance of fibrosis in association with genetic defects may impair propagation of the impulse through the conduction system. In some PCCD patients, a conduction defect is documented from birth. Depending on the consequence of the mutation on the sodium channels, the phenotype may be progressive or congenital (**Table**).[4]

If the action potential generation and/or propagation is more severely impaired in the atria than in the ventricles in *SCN5A* mutation patients, the sinus node dysfunction caused by failure of the impulses to conduct into the adjacent atrial myocardium (exit block) has been suggested as a cause of SSS, atrial standstill, and atrial fibrillation (**Table**).[5]

Mutations of E1784K in *SCN5A* cause a persistent (late) inward Na^+ current, and also cause a reduction in the peak Na^+ current.[9,11,12] Some LQT3 patients present with ECG findings characteristic of BrS (overlap syndrome), and one of the causes of this overlapping syndrome can be explained by E1784K,[11,12] 1795insD,[13,14] ΔKPQ,[12,15] and ΔK1500.[16] However, several other biophysical mechanisms may be related to the reduction in the peak Na current.[17]

Sodium-channel blockers are commonly used in patients with LQT3 because of the blocking effect on persistent Na currents.[18–20] However, in overlap syndrome, sodium-channel blockers shorten the QT interval, possibly reducing the peak Na current, and thus uncover a concealed BrS resulting in typical ST segment elevation in the right precordial leads, and may provoke malignant ventricular arrhythmias.[14]

In this issue of the Journal, Takahashi et al report that the E1784K mutation in *SCN5A* is the most prevalent mutation in school children with LQTS in the Okinawa islands.[21] The most common mutation in LQTS is reported to be a *KCNQ1* mutation.[22,23] It is noteworthy that there is a high prevalence rate of

Table. *SCN5A* Mutations and Associated Inherited Arrhythmias

Syndrome	Phenotype	Possible cause of the syndrome
LQT3	Prolonged QT	Persistent Na current
BrS	RBBB type QRS, ST elevation in the right precordial leads	Reduction in the initial opening of the Na channels in the epicardial right ventricular outflow tract cells
PCCD	BBB, AVB	Fibrosis and conduction disturbance of the conduction system
SSS	Sinus bradycardia, SA block	Failure of conduction from the sinus node (exit block), morphological changes in the atrial cells
Atrial standstill	Junctional rhythm without P waves	Failure of conduction in the atrium
AF	AF	Morphological changes of the atrial cells
Overlap syndrome	LQT3, BrS, SSS	Persistent Na current and reduction in the initial Na current

AF, atrial fibrillation; AVB, AV block; BBB, bundle branch block; BrS, Brugada syndrome; LQT3, long QT type 3; PCCD, progressive cardiac conduction system disturbance; RBBB, right bundle branch block; SA block, sino-atrial block; SSS, sick sinus syndrome.

Received May 18, 2014; accepted May 18, 2014; released online June 10, 2014

Department of Pediatric Cardiology, Saitama Medical University International Medical Center, Hidaka, Japan
Mailing address: Naokata Sumitomo, MD, PhD, Department of Pediatric Cardiology, Saitama Medical University International Medical Center, 1397-1 Yamane, Hidaka 350-1298, Japan. E-mail: sumitomo@saitama-med.ac.jp

ISSN-1346-9843 doi:10.1253/circj.CJ-14-0564

LQT3 (63%) in the Okinawa islands, and all the mutations are E1784K in *SCN5A*.[21] From this result, the ancestors of the Okinawa islands may differ from those of the other islands in Japan. As reported, BrS is much more prevalent in the Asian region,[24] and we need to investigate the prevalence of LQT3 incidence and also E1784K mutations in *SCN5A*.

In the study by Takahashi et al,[21] one in 8 of the phenotypes was revealed to have the BrS-type ST elevation while taking mexiletine. Those patients may have an overlapping syndrome of LQT3 and BrS. A closer look at the ST changes in the right precordial leads and 3rd intercostal space right precordial lead recording may be needed when an LQT3 gene anomaly is found, especially an E1784K mutation in *SCN5A*. Further, great care also must be taken when using sodium-channel blockers and β-blockers in patients with LQT3.

References

1. Keating MT. The long QT syndrome: A review of recent molecular genetic and physiologic discoveries. *Medicine* 1996; **75:** 1–5.
2. Bennett PB, Yazawa K, Makita N, George AL Jr. Molecular mechanism for an inherited cardiac arrhythmia. *Nature* 1995; **376:** 683–685.
3. Chen Q, Kirsch GE, Zhang D, Brugada R, Brugada J, Brugada P, et al. Genetic basis and molecular mechanism for idiopathic ventricular fibrillation. *Nature* 1998; **392:** 293–296.
4. Schott JJ, Alshinawi C, Kyndt F, Probst V, Hoorntje TM, Hulsbeek M, et al. Cardiac conduction defects associate with mutations in SCN5A. *Nat Genet* 1999; **23:** 20–21.
5. Benson DW, Wang DW, Dyment M, Knilans TK, Fish FA, Strieper MJ, et al. Congenital sick sinus syndrome caused by recessive mutations in the cardiac sodium channel gene (SCN5A). *J Clin Invest* 2003; **112:** 1019–1028.
6. Ziyadeh-Isleem A, Clatot J, Duchatelet S, Gandjbakhch E, Denjoy I, Hidden-Lucet F, et al. A truncating SCN5A mutation combined with genetic variability causes sick sinus syndrome and early atrial fibrillation. *Heart Rhythm* 2014 February 25, doi:10.1016/j.hrthm.2014.02.021.
7. Wilde AA, Brugada R. Phenotypical manifestations of mutations in the genes encoding subunits of the cardiac sodium channel. *Circ Res* 2011; **108:** 884–897.
8. Remme CA, Wilde AAM, Bezzina CR. Cardiac sodium channel overlap syndromes: Different faces of SCN5A mutations. *Trend Cardiovasc Med* 2008; **18:** 78–87.
9. Makita N. Phenotypic overlap of cardiac sodium channelopathies: Individual-specific or mutation-specific? *Circ J* 2009; **73:** 810–817.
10. Kato K, Makiyama T, Wu J, Ding WG, Kimura H, Naiki N, et al. Cardiac channelopathies associated with infantile fatal ventricular arrhythmias: From the cradle to the bench. *J Cardiovasc Electrophysiol* 2014; **25:** 66–73.
11. Makita N, Behr E, Shimizu W, Horie M, Sunami A, Crotti L, et al. The E1784K mutation in SCN5A is associated with mixed clinical phenotype of type 3 long QT syndrome. *J Clin Invest* 2008; **118:** 2219–2229.
12. Priori SG, Napolitano C, Schwartz PJ, Bloise R, Crotti L, Ronchetti E. The elusive link between LQT3 and Brugada syndrome: The role of flecainide challenge. *Circulation* 2000; **102:** 945–947.
13. Veldkamp MW, Viswanathan PC, Bezzina C, Baartscheer A, Wilde AA, Balser JR. Two distinct congenital arrhythmias evoked by a multidysfunctional Na^+ channel. *Circ Res* 2000; **86:** E91–E97, doi:10.1161/01.RES.86.9.e91.
14. Bezzina C, Veldkamp MW, van Den Berg MP, Postma AV, Rook MB, Viersma JW, et al. A single Na^+ channel mutation causing both long-QT and Brugada syndromes. *Circ Res* 1999; **85:** 1206–1213.
15. Moss AJ, Windle JR, Hall WJ, Zareba W, Robinson JL, McNitt S, et al. Safety and efficacy of flecainide in subjects with long QT-3 syndrome (ΔKPQ mutation): A randomized, double-blind placebo-controlled clinical trial. *Ann Noninvasive Electrocardiol* 2005; **10:** 59–66.
16. Grant AO, Carboni MP, Neplioueva V, Starmer CF, Memmi M, Napolitano C, et al. Long QT syndrome, Brugada syndrome, and conduction system disease are linked to a single sodium channel mutation. *J Clin Invest* 2002; **110:** 1201–1209.
17. Antzelevitch C. The Brugada syndrome: Ionic basis and arrhythmia mechanisms. *J Cardiovasc Electrophysiol* 2001; **12:** 268–272.
18. Schwartz PJ, Priori SG, Locati EH, Napolitano C, Cantù F, Towbin JA, et al. Long QT syndrome patients with mutations of the SCN5A and HERG genes have differential responses to Na^+ channel blockade and to increases in heart rate: Implications for gene-specific therapy. *Circulation* 1995; **92:** 3381–3386.
19. Benhorin J, Taub R, Goldmit M, Kerem B, Kass RS, Windman I, et al. Effects of flecainide in patients with new SCN5A mutation: Mutation specific therapy for long-QT syndrome? *Circulation* 2000; **101:** 1698–1706.
20. Schwartz PJ. The congenital long QT syndromes from genotype to phenotype: Clinical implications. *J Intern Med* 2006; **259:** 39–47.
21. Takahashi K, Shimizu W, Miyake A, Nabeshima T, Nakayashiro M, Ganaha H. High prevalence of the *SCN5A* E1784K mutation in school children with long QT syndrome living on the Okinawa Islands. *Circ J* 2014 May 28, doi:10.1253/circj.CJ-13-1516 [Epub ahead of print].
22. Splawski I, Shen J, Timothy KW, Lehmann MH, Priori S, Robinson JL, et al. Spectrum of mutations in long-QT syndrome genes: KVLQT1, HERG, SCN5A, KCNE1, and KCNE2. *Circulation* 2000; **102:** 1178–1185.
23. Napolitano C, Priori SG, Schwartz PJ, Bloise R, Ronchetti E, Nastoli J, et al. Genetic testing in the long QT syndrome: Development and validation of an efficient approach to genotyping in clinical practice. *JAMA* 2005; **294:** 2975–2980.
24. Murakoshi N, Aonuma K. Epidemiology of arrhythmias and sudden cardiac death in Asia. *Circ J* 2013; **77:** 2419–2431.

Efficacy and safety of flecainide for ventricular arrhythmias in patients with Andersen-Tawil syndrome with *KCNJ2* mutations

Koji Miyamoto, MD,[*†] Takeshi Aiba, MD, PhD,[*] Hiromi Kimura, MD, PhD,[‡] Hideki Hayashi, MD, PhD,[‡] Seiko Ohno, MD, PhD,[‡] Chie Yasuoka, MD, PhD,[§] Yoshihito Tanioka, MD, PhD,[§] Takeshi Tsuchiya, MD, PhD,[‖] Yoko Yoshida, MD,[¶] Hiroshi Hayashi, MD,[#] Ippei Tsuboi, MD,[#] Ikutaro Nakajima, MD,[*] Kohei Ishibashi, MD,[*] Hideo Okamura, MD,[*†] Takashi Noda, MD, PhD,[*] Masaharu Ishihara, MD, PhD,[*†] Toshihisa Anzai, MD, PhD,[*†] Satoshi Yasuda, MD, PhD,[*†] Yoshihiro Miyamoto, MD, PhD,[**] Shiro Kamakura, MD, PhD,[*] Kengo Kusano, MD, PhD,[*†] Hisao Ogawa, MD, PhD,[*††] Minoru Horie, MD, PhD,[‡] Wataru Shimizu, MD, PhD[*†#]

From the [*]Department of Cardiovascular Medicine, National Cerebral and Cardiovascular Center, Suita, Japan, [†]Department of Advanced Cardiovascular Medicine, Graduate School of Medical Sciences, Kumamoto University, Kumamoto, Japan, [‡]Department of Cardiovascular and Respiratory Medicine, Shiga University of Medical Science, Otsu, Japan, [§]Department of Cardiology, Omura Municipal Hospital, Omura, Japan, [‖]EP Expert Doctors-Team Tsuchiya, Kumamoto, Japan, [¶]Department of Pediatric Electrophysiology, Osaka City General Hospital, Osaka, Japan, [#]Department of Cardiovascular Medicine, Nippon Medical School, Tokyo, Japan, [**]Department of Preventive Cardiology, National Cerebral and Cardiovascular Center, Suita, Japan, and [††]Department of Cardiovascular Medicine, Graduate School of Medical Sciences, Kumamoto University, Kumamoto, Japan.

BACKGROUND Andersen-Tawil syndrome (ATS) is an autosomal dominant genetic or sporadic disorder characterized by ventricular arrhythmias (VAs), periodic paralyses, and dysmorphic features. The optimal pharmacological treatment of VAs in patients with ATS remains unknown.

OBJECTIVE We evaluated the efficacy and safety of flecainide for VAs in patients with ATS with *KCNJ2* mutations.

METHODS Ten ATS probands (7 females; mean age 27 ± 11 years) were enrolled from 6 institutions. All of them had bidirectional VAs in spite of treatment with β-blockers (n = 6), but none of them had either aborted cardiac arrest or family history of sudden cardiac death. Twenty-four-hour Holter recording and treadmill exercise test (TMT) were performed before (baseline) and after oral flecainide therapy (150 ± 46 mg/d).

RESULTS Twenty-four-hour Holter recordings demonstrated that oral flecainide treatment significantly reduced the total number of VAs (from 38,407 ± 19,956 to 11,196 ± 14,773 per day; $P = .003$) and the number of the longest ventricular salvos (23 ± 19 to 5 ± 5; $P = .01$). At baseline, TMT induced nonsustained ventricular tachycardia (n = 7) or couplets of premature ventricular complex (n = 2); treatment with flecainide completely (n = 7) or partially (n = 2) suppressed these exercise-induced VAs ($P = .008$). In contrast, the QRS duration, QT interval, and U-wave amplitude of the electrocardiogram were not altered by flecainide therapy. During a mean follow-up of 23 ± 11 months, no patients developed syncope or cardiac arrest after oral flecainide treatment.

CONCLUSION This multicenter study suggests that oral flecainide therapy is an effective and safe means of suppressing VAs in patients with ATS with *KCNJ2* mutations, though the U-wave amplitude remained unchanged by flecainide.

KEYWORDS Andersen-Tawil syndrome; Long QT; Flecainide; Ventricular arrhythmia; Mutation

ABBREVIATIONS APD = action potential duration; **ATS** = Andersen-Tawil syndrome; **CPVT** = catecholaminergic polymorphic ventricular tachycardia; **ECG** = electrocardiogram/electrocardiographic; $\mathbf{I_{K1}}$ = inward rectifying K^+ current; **QTc interval** = corrected QT interval by Bazett's formula; **QUc interval** = corrected QU interval by Bazett's formula; **RyR2** = ryanodine receptor 2; **TMT** = treadmill exercise test; **VA** = ventricular arrhythmia; **VT** = ventricular tachycardia

(Heart Rhythm 2015;12:596–603)

This work was supported by a Grant-in-Aid for Scientific Research on Innovative Areas (grant no. 22136011 A02, to Dr Aiba), a Grant-in-Aid for Scientific Research (C) (grant no. 24591086, to Dr Aiba) from the Ministry of Education, Culture, Sports, Science and Technology (MEXT) of Japan, and a Research Grant for Cardiovascular Diseases (grant nos. H24-033 and H26-040, to Dr Aiba, Dr Miyamoto, Dr Kamakura, Dr Horie, and Dr Shimizu) from the Ministry of Health, Labor and Welfare, Japan. **Address reprint requests and correspondence:** Dr Takeshi Aiba, Division of Arrhythmia and Electrophysiology, Department of Cardiovascular Medicine, National Cerebral and Cardiovascular Center, 5-7-1, Fujishiro-dai, Suita, Osaka 565-8565, Japan. E-mail address: aiba@hsp.ncvc.go.jp. Dr Wataru Shimizu, Department of Cardiovascular Medicine, Nippon Medical School, 1-1-5 Sendagi, Bunkyo-ku, Tokyo 113-8603, Japan. E-mail address: wshimizu@nms.ac.jp.

1547-5271/$-see front matter http://dx.doi.org/10.1016/j.hrthm.2014.12.009

Introduction

Andersen-Tawil syndrome (ATS) is a heterogeneous, autosomal dominant genetic or sporadic disorder characterized by ventricular arrhythmias (VAs), periodic paralyses, and dysmorphic features.[1,2] ATS is a channelopathy linked to mutations in the *KCNJ2* gene encoding the α subunit of Kir2.1.[3–6] Patients with ATS often have a variety of VAs such as premature ventricular complex, polymorphic ventricular tachycardia (VT), and bidirectional VT. Although the cycle length of VAs in patients with ATS is relatively long and fatal cardiac event is rare, VAs often occur and lead to symptoms such as syncope and palpitations.[7] Moreover, sudden cardiac death and tachycardia-induced cardiomyopathy in patients with ATS have also been reported.[8,9] Thus, VA suppression is clinically important for patients with ATS.

Although β-blockers and calcium channel blockers have been used to treat VAs in patients with ATS,[7,10–12] these drugs do not sufficiently suppress VAs. As an alternative, empirical case reports[7,8,13] have suggested that flecainide might be effective for the suppression of VAs in patients with ATS. To date, however, there are few systematic evaluations of oral flecainide as a treatment of VAs in patients with ATS. Accordingly, this study aimed to assess the efficacy and safety of flecainide for VAs in patients with ATS with *KCNJ2* mutations.

Methods

Study population

The study population consisted of 10 unrelated ATS probands from 6 institutions in Japan who were treated with oral flecainide. We prospectively enrolled patients with ATS who were expected to use flecainide as a treatment of VAs. Patients who could not perform treadmill exercise test (TMT) and were more than 80 years old were excluded from this study. ATS was diagnosed on the basis of clinical features such as VAs, episodes of periodic paralysis, and/or dysmorphic features as well as the presence of *KCNJ2* genetic mutations. Cardiac involvement was determined on the basis of the presence of VAs (premature ventricular complex, polymorphic VT, and/or bidirectional VT), prolongation of the corrected QT (QU) interval (QTc [QUc] interval), and/or enlargement of the U wave on a 12-lead electrocardiogram (ECG).[1–6] The periodic paralysis was diagnosed according to the standard criteria.[14] Dysmorphology was defined as the presence of 2 or more of the following: (1) low-set ears, (2) hypertelorism, (3) small mandible, (4) clinodactyly, and (5) syndactyly.[4]

To evaluate the efficacy of flecainide, 24-hour Holter recording and TMT were performed in all patients before (baseline) and after flecainide therapy. Dose of flecainide was determined by the physician who treated the patient in this study. Physicians usually administered 2–3 mg/kg of flecainide and titrated according to the result of Holter recording, TMT, blood concentration of flecainide, and patient intention. All participants provided written informed consent according to the protocol approved by the institutional review board (M24-028-2).

Twelve-lead ECG

A 12-lead ECG was recorded at a paper speed of 25 mm/s during sinus rhythm in all patients in the supine resting state. The R-R, PR, QT, QU, and Tpeak-Upeak intervals as well as QRS duration were measured. The QT interval was defined as the period from the onset of the QRS complex to the end of the T wave. The U wave was defined as an early diastolic deflection after the end of the T wave,[15] and an enlarged U wave was defined according to the following criteria: (1) wave amplitude ≥ 0.2 mV or (2) amplitude larger than the preceding T wave. T-wave and U-wave durations were defined as the periods from the onset of the T wave and U wave to the end of the T wave and U wave, respectively.[15] The end of the T wave and that of the U wave were the points at which tangents drawn to the steepest downslopes of the T wave and U wave, respectively, crossed the isoelectric line. T-wave and U-wave amplitudes and durations were also measured. The QU interval was defined as the period from the onset of the QRS complex to the end of the U wave. The amplitude of the T wave or U wave was measured at each highest amplitude lead, whereas the U/T-wave ratio was calculated at the highest amplitude U-wave lead. The QT and QU intervals were corrected by applying Bazett's formula (QTc and QUc intervals, respectively).[6] Polymorphic VT was defined as a VT with an irregularly variable axis of the QRS complex. Bidirectional VT was defined as a VT with a beat-to-beat alternation of the QRS axis.[16]

Mutation analysis

The protocol for genetic analysis was approved by the institutional ethics committee and performed under its guidelines (M24-031-4). All patients provided informed consent before the genetic analysis. Genomic DNA was isolated from whole blood using a DNA analyzer (QIAGEN GmbH, Hilden, Germany).[17] Genetic screening for *KCNJ2* was performed by using the direct sequencing method (ABI 3730 DNA Analyzer, Life Technologies, Carlsbad, CA). The complementary DNA sequence numbering was based on the GenBank reference sequence NM_000891.2 for *KCNJ2*.

Holter recording

A 24-hour Holter recording was performed in all patients before and after flecainide therapy. The following parameters were used to assess the clinical efficacy and safety of flecainide: (1) total number of VAs, (2) number of the longest ventricular salvos and cycle length during the VT, and (3) number of episodes of VT (≥3 successive VAs).

TMT

The TMT using a standard or modified Bruce protocol was performed before and after the initiation of flecainide therapy. The following parameters were used to assess the clinical efficacy of flecainide: (1) number of the longest